p27^{Kip1} promotes invadopodia turnover and invasion through the regulation of the PAK1/Cortactin pathway

Pauline Jeannot[1,2,3], Ada Nowosad[1,2,3], Renaud T Perchey[1,2,3], Caroline Callot[1,2,3], Evangeline Bennana[4], Takanori Katsube[5], Patrick Mayeux[4], François Guillonneau[4], Stéphane Manenti[1,2,3], Arnaud Besson[1,2,3]*

[1]INSERM UMR1037, Cancer Research Center of Toulouse, Toulouse, France; [2]Université Toulouse III Paul Sabatier, Toulouse, France; [3]CNRS ERL5294, Toulouse, France; [4]3P5 proteomics facility of the Université Paris Descartes, Inserm U1016 Institut Cochin, Sorbonne Paris Cité, Paris, France; [5]National Institute of Radiological Sciences, Chiba, Japan

Abstract p27^{Kip1} (p27) is a cyclin-CDK inhibitor and negative regulator of cell proliferation. p27 also controls other cellular processes including migration and cytoplasmic p27 can act as an oncogene. Furthermore, cytoplasmic p27 promotes invasion and metastasis, in part by promoting epithelial to mesenchymal transition. Herein, we find that p27 promotes cell invasion by binding to and regulating the activity of Cortactin, a critical regulator of invadopodia formation. p27 localizes to invadopodia and limits their number and activity. p27 promotes the interaction of Cortactin with PAK1. In turn, PAK1 promotes invadopodia turnover by phosphorylating Cortactin, and expression of Cortactin mutants for PAK-targeted sites abolishes p27's effect on invadopodia dynamics. Thus, in absence of p27, cells exhibit increased invadopodia stability due to impaired PAK1-Cortactin interaction, but their invasive capacity is reduced compared to wild-type cells. Overall, we find that p27 directly promotes cell invasion by facilitating invadopodia turnover via the Rac1/PAK1/Cortactin pathway.

DOI: 10.7554/eLife.22207.001

*For correspondence: arnaud. besson@inserm.fr

Introduction

p27^{Kip1} is a cell cycle inhibitor that binds to a broad range of cyclin-CDK complexes (*Besson et al., 2008*). p27-mediated cyclin-CDK inhibition involves the N-terminal extremity (aa 28–89) of the protein that allows interaction with both cyclin and CDK subunits (*Ou et al., 2012*; *Besson et al., 2008*). The critical role of p27 as a negative regulator of cell proliferation is underscored by the phenotype of p27 knockout mice, which exhibit a hyperproliferative phenotype in multiple tissues and are more susceptible to tumor development than wild-type animals (*Fero et al., 1996*; *Kiyokawa et al., 1996*; *Nakayama et al., 1996*; *Besson et al., 2006*; *Fero et al., 1998*). While the tumor suppressive role of p27 is confirmed by the frequent loss of p27 expression in many types of cancers, p27 is also mislocalized in a fraction of tumors due to activation of various signaling pathways that cause its nuclear export and/or cytoplasmic retention (*Chu et al., 2008*). Cytoplasmic p27 has been associated with decreased patient survival, high tumor grade and metastasis in several tumor types including breast carcinomas, acute myeloid leukemia, glioblastoma, melanoma and non-small cell lung carcinomas (*Lin et al., 2016*; *Chu et al., 2008*; *Liang et al., 2002*; *Yang et al., 2011*; *Min et al., 2004*; *Cheng et al., 2015*). The possibility that cytoplasmic p27 may confer a pro-tumorigenic advantage was confirmed in a mouse model expressing a mutant form of p27 that cannot bind cyclin-CDK complexes (p27CK-) (*Besson et al., 2007*; *Serres et al., 2011*). These mice are more

eLife digest When animals develop from embryos to adults, or try to heal wounds later in life, their cells have to move. Moving means that the cells must invade into their surroundings, a dense network of proteins called the extracellular matrix. The cell first attaches to the extracellular matrix; degrades it; and then moves into the newly opened space. Cells have developed specialized structures called invadosomes to enable all these steps. Invadosomes are never static, they first assemble where cells interact with extracellular matrix, they then release proteins that loosen the matrix, and finally disassemble again to allow cells to move. Invadosomes in cancer cells often become overactive, and can allow the tumor cells to spread throughout the body.

A lot of different proteins are involved in controlling how and when cells move. p27 is a well-known protein usually found in a cell's nucleus along with the cell's DNA. Inside the nucleus, p27 suppresses tumor growth by stopping cells from dividing. However, often in cancer cells p27 moves outside of the cell's nucleus where it contributes to cell movement via an unknown mechanism.

To answer how p27 controls cell invasion, Jeannot et al. used a biochemical technique to uncover which proteins p27 binds to when it is outside of the nucleus. One of its interaction partners was called Cortactin. This protein is known to be an important building block of invadosomes, and is involved in both the assembly and disassembly of these structures. In further experiments, Jeannot studied mouse cells with or without p27 and human cancer cells that can be grown in the laboratory. The experiments revealed that p27 promotes an enzyme called PAK1 to also bind to Cortactin. PAK1 then modified Cortactin, causing whole invadosomes to disassemble, which in turn allowed cells to de-attach from the matrix and move forward. In contrast, cells lacking p27 had more stable invadosomes, attached more strongly to the matrix and were better at degrading it, but could not invade as well as cells with p27.

Overall these experiments showed a new way that p27 promotes cell invasion. The next steps will include finding out exactly how the modification of Cortactin causes the invadosomes to disassemble. Furthermore, it will be important to study whether forcing p27 back into the nucleus can reduce the spread of cancer cells in the body.

susceptible than p27-null and wild-type mice to both spontaneous and induced tumor development, thus uncovering an oncogenic role for p27 in vivo (*Serres et al., 2011*; *Besson et al., 2007*).

It now appears that p27 is a multifunctional protein involved in the regulation of multiple cellular processes, some of which are regulated by p27 in a CDK-independent manner (*Besson et al., 2008*; *Sharma and Pledger, 2016*). Indeed, p27 has been implicated in the control of cell migration, transcriptional repression, autophagy, stem cell specification and differentiation, cytokinesis, and apoptosis (*Besson et al., 2008*; *Sharma and Pledger, 2016*; *Baldassarre et al., 2005*; *Besson et al., 2004b, 2007*; *Pippa et al., 2012*; *Serres et al., 2012*; *Nickeleit et al., 2008*; *Liang et al., 2007*; *Li et al., 2012*; *Nguyen et al., 2006*; *Jeannot et al., 2015*). This functional versatility may stem from the intrinsically disordered structure of p27, which folds upon binding to other proteins, allowing p27 to interact with a wide variety of partners (*Lacy et al., 2004*; *Galea et al., 2008*). While these various functions participate in homeostasis in normal cells and tissues, they may be co-opted by tumor cells to promote oncogenesis.

Metastasis, the process whereby cells from a primary tumor disseminate throughout the body and form secondary tumors at distant sites, is the leading cause of cancer related death (*Sethi and Kang, 2011*). It requires tumor cells to migrate and invade through neighboring tissues, enter the blood flow and then extravasate to disseminate and form new tumors in host tissues (*Sethi and Kang, 2011*). Regulation of cell motility was the first CDK-independent role ascribed to p27 (*Nagahara et al., 1998*; *Denicourt et al., 2007*; *Besson et al., 2004b*). In the cytosol, p27 can interact with RhoA, preventing RhoA activation by guanine-nucleotide exchange factors (GEFs) and thereby modulating actin cytoskeleton dynamics and migration (*Besson et al., 2004a, 2004b*). Consequently, mouse embryo fibroblasts (MEFs) lacking p27 have more RhoA activity, increased numbers of stress fibers and focal adhesions and exhibit a defect in migration (*Besson et al., 2004b*). This pathway is important for proper migration of bone marrow

macrophages and developing cortical neurons and for cancer cell migration and invasion in vivo (*Godin et al., 2012*; *Nguyen et al., 2006*; *Papakonstanti et al., 2007*; *Gui et al., 2014*; *Wu et al., 2006*; *See et al., 2010*; *Larrea et al., 2009*; *Jin et al., 2013*). p27 can also regulate cell migration by controlling microtubule stability through Stathmin or directly by binding to microtubules and promoting microtubule polymerization (*Baldassarre et al., 2005*; *Godin et al., 2012*). In a 3D environment, cells adopt different strategies to migrate and invade through surrounding matrix (*Petrie and Yamada, 2016*; *Sethi and Kang, 2011*). The mode of migration is influenced, at least in part, by the activities of Rho GTPases: RhoA activity favors an amoeboid migration, whereas Rac1 activity promotes mesenchymal migration (*Sahai and Marshall, 2003*; *Vial et al., 2003*). Accordingly, cytoplasmic p27 promotes mesenchymal migration via the inhibition of RhoA activity, while cells lacking p27 tend to adopt an amoeboid mode of migration (*Gui et al., 2014*; *Belletti et al., 2010*). More recently, p27 was reported to promote epithelial to mesenchymal transition by binding to JAK2, promoting STAT3 activation and the upregulation of Twist1 (*Zhao et al., 2015*).

Here, we describe a novel mechanism by which p27 directly regulates invadopodia formation and cell invasion through extracellular matrix (ECM) via Cortactin. Invadosomes (designating both invadopodia and podosomes) are thought to allow cells to coordinate ECM degradation with migration within the tissue microenvironment (*Murphy and Courtneidge, 2011*; *Linder et al., 2011*; *Di Martino et al., 2016*). Cortactin plays a key role in the formation of actin protrusive structures such as lamellipodia and invadosomes (*Murphy and Courtneidge, 2011*; *Kirkbride et al., 2011*; *MacGrath and Koleske, 2012*). Cortactin has been involved in all steps of the invadosome lifecycle, from assembly, maturation, proteolytic activity and disassembly (*MacGrath and Koleske, 2012*; *Murphy and Courtneidge, 2011*; *Moshfegh et al., 2014*). All these steps appear to be regulated by phosphorylation events on Cortactin (*Oser et al., 2009*; *Moshfegh et al., 2014*; *Murphy and Courtneidge, 2011*). Overall, Cortactin is a scaffold protein composed of an N-terminal acidic domain, followed by several actin-binding repeats allowing its interaction with F-actin, a Pro-rich region and a SH3 domain (*MacGrath and Koleske, 2012*; *Kirkbride et al., 2011*). Phosphorylation of Cortactin by Src and Abl family tyrosine kinases has two effects: first, this releases the actin severing protein Cofilin from an inhibitory interaction with Cortactin and generates actin barbed ends; second, Arp2/3, N-WASP and Nck1 are recruited onto Cortactin, promoting the polymerization of branched actin (*Oser et al., 2009*; *Weaver et al., 2002*; *Oser et al., 2010*). Dephosphorylation of Cortactin then allows the inhibition of Cofilin activity and stabilizes the invadopodia (*Oser et al., 2009*). Cortactin also plays a key role in matrix metalloproteinase secretion in mature invadopodia (*Clark et al., 2007*). Finally, invadopodia disassembly is induced by sequential activation of the Rac-GEF Trio, Rac1 and p21-Activated Kinase-1 (PAK1) pathway and presumably by PAK1-mediated phosphorylation of Cortactin on Ser113, since a Ser113 to Ala mutant blocked invadopodia disassembly (*Moshfegh et al., 2014*). How PAK-phosphorylated Cortactin mediates invadopodia disassembly is still unclear but could be due, at least in part, to a decreased affinity of Cortactin phosphorylated within its F-actin binding repeats (on S113, S150 and/or S282) for F-actin, potentially destabilizing the structure (*Webb et al., 2006, 2005*).

We found that p27 binds to Cortactin and localizes to invadopodia following serum or growth factor stimulation and promotes cell invasion. Paradoxically, p27-null cells have more invadopodia and degrade gelatin more efficiently, but exhibit impaired invasive capacity. In fact, we found that p27 promotes the recruitment of PAK1 to Cortactin and invadopodia turnover and this is dependent on phosphorylation of S113/S150/S282 of Cortactin, the sites targeted by PAK kinases. Thus, in absence of p27, the dynamics of invadopodia is altered and prevents efficient invasion through ECM. Altogether, we have identified a novel mechanism by which p27 directly controls cell invasion that could contribute to the increased invasive and metastatic capacity of tumors where p27 is mislocalized in the cytoplasm.

Results

p27 interacts with Cortactin and localizes to invadopodia

While the role of p27 in the regulation of cell migration is firmly established, how p27 is targeted to specific locations in the cytoplasm to control motility and invasion remains unclear (*Gui et al., 2014*; *Belletti et al., 2010*; *Besson et al., 2004a, 2004b*; *Godin et al., 2012*; *Nguyen et al., 2006*;

Papakonstanti et al., 2007; *Wu et al., 2006*; *See et al., 2010*; *Larrea et al., 2009*; *Jin et al., 2013*). We recently identified Cortactin in a proteomic screen in which protein arrays (Protoarray, Thermo-Fisher Scientific) were probed with recombinant human p27, indicating that the two proteins interact directly. We confirmed the binding of p27 to Cortactin in HEK 293 cells overexpressing p27 and Myc-tagged Cortactin (*Figure 1A*), as well as on endogenous proteins in Hela cells and MEFs immortalized with the human papilloma virus E6 protein (*Figure 1B*) (*Serres et al., 2011*). The interaction domain of Cortactin on p27 was mapped by pull-down assays using various GST-p27 fusion proteins and Myc-Cortactin in HEK 293 cells. Cortactin bound to the p27CK- mutant, that cannot interact with cyclins and CDKs (*Besson et al., 2006*, *2007*), and to the C-terminal half (aa 88–198) of p27 but not the N-terminal half (aa 1–87) of the protein that contains the cyclin and CDK interaction domains (*Figure 1C and D*). The Cortactin interaction domain on p27 was narrowed down to the last 8 aa of p27, as a p27CK- 1–190 mutant did not interact with Cortactin any longer (*Figure 1E*). A p27CK- 1–197 mutant, lacking only the C-terminal threonine residue, still bound to Cortactin (*Figure 1E*), suggesting that phosphorylation on T198 is not needed for binding to Cortactin.

Similarly, pull-down assays using full-length GST-p27 were performed on HEK 293 cell lysates expressing various Myc-tagged Cortactin truncation mutants to map the p27 interaction domain on Cortactin (*Katsube et al., 2004*). These experiments revealed that p27 interacts with the N-terminal half of Cortactin, within the actin binding repeats, as a mutant Cortactin lacking the actin binding repeats 3 to 6 (ΔABR3-6) did not bind p27 (*Figure 1F*).

Since Cortactin is a key component of invadopodia, we determined if p27 could colocalize with Cortactin in these structures. To remove most of soluble p27 prior to fixation and immunostaining, p27+/+E6 MEFs were permeabilized with digitonin, as described previously (*Serres et al., 2012*). In these conditions, p27 could be readily observed in invadopodia where it colocalized with Tks5, a commonly used invadopodia marker (*Seals et al., 2005*), or Cortactin (*Figure 2A and B*, respectively). The same approach was used to confirm p27 localization to invadopodia in human A549 lung adenocarcinoma and A375 melanoma cell lines (*Figure 2—figure supplement 1*).

Invadopodium and podosome formation is stimulated by growth factors (*Murphy and Courtneidge, 2011*). Growth factor stimulation causes the degradation of p27 as cells enter the cell cycle but also the relocalization of a fraction of p27 in the cytoplasm between 1 hr and 6 hr post-stimulation, dependent on the phoshorylation of p27 on Ser10 (*Besson et al., 2006*, *2004b*; *Boehm et al., 2002*; *Ishida et al., 2002*; *Rodier et al., 2001*; *Connor et al., 2003*). Consistent with the translocation of p27 in the cytoplasm and the formation of invadopodia after serum or growth factor stimulation, an increased association between p27 and Cortactin by co-immunoprecipitation at 1 hr and 3 hr post-stimulation in p27+/+E6 MEFs (*Figure 2C*) and in Hela cells (*Figure 2—figure supplement 2*) was observed in five and three independent experiments, respectively. However, due to variability in signal intensities among independent experiments, these differences were not statistically significant. Together, our data indicate that a fraction of cytoplasmic p27 localizes to invadopodia after growth factor stimulation, where it binds to Cortactin.

p27 regulates invadopodia formation and promotes invasion

Invadopodia and podosomes are capable of both adhering to and degrading ECM (*Murphy and Courtneidge, 2011*; *Di Martino et al., 2016*). Fibroblasts do not normally form invadosomes unless transformed by Src (*Murphy and Courtneidge, 2011*). We first verified that the E6 immortalized MEF lines used in our study were forming functional, matrix degrading invadopodia. For this, p27+/+, p27−/− and p27CK-/CK- E6 MEFs were seeded on fluorescent gelatin and Tks5 immunostaining indicated that these cells could all form Tks5-containing structures that efficiently degraded gelatin (*Figure 3—figure supplement 1*). p27 colocalized with Tks5 at sites of gelatin degradation in MEFs and A549 cells, suggesting that p27 can be present at functional invadopodia (*Figure 3—figure supplement 2*). Since p27 binds to Cortactin and can localize to invadopodia, we determined if p27 status influenced the ability of cells to form invadopodia. Counting of the number of cells forming invadopodia using Tks5 immunostaining (*Figure 3A*) revealed that while cells expressing p27 or p27CK- rarely formed invadopodia (5.83% and 8.68%, respectively), nearly half of MEFs lacking p27 had invadopodia (44.66%) (*Figure 3B*). In keeping with the number of invadopodia forming cells, measurement of the area of fluorescent gelatin degraded per cell showed that p27−/− cells had a dramatically increased capacity to degrade ECM compared to p27+/+ and p27CK-/CK- MEFs (*Figure 3C and D*).
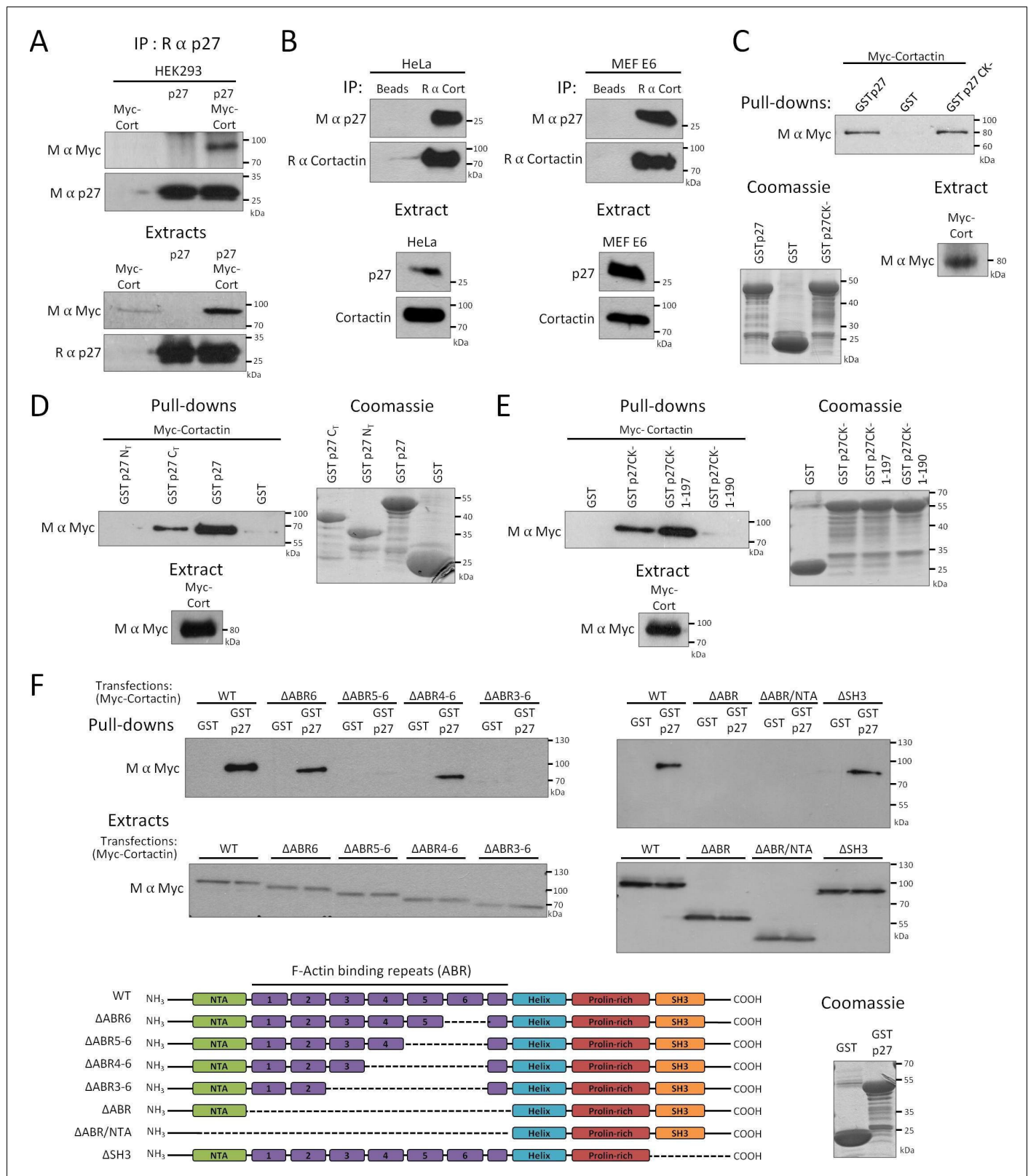
Figure 1. p27 binds to Cortactin. (**A–B**) Co-immunoprecipitation of p27 and Cortactin: (**A**) p27 was immunoprecipitated using rabbit anti-p27 (C19) antibodies from HEK293 lysates transfected with plasmids encoding p27, Myc-Cortactin (Myc-Cort) or both. (**B**) Immunoprecipitation of endogenous Cortactin using rabbit anti-Cortactin (H191) antibodies from HeLa or E6 MEF lysates, beads alone were used as control. (**A–B**) Co-immunoprecipitated proteins were detected by immunoblot with mouse anti-c-Myc (9E10) (**A**) or mouse anti-p27 (F-8) antibodies (**B**). Immunoprecipitated proteins were

Figure 1 continued on next page

Figure 1 continued

visualized by reprobing the membrane with mouse anti-p27 (F-8) (**A**) or with rabbit anti-Cortactin (H-191) antibodies and anti-rabbit Ig light-chain secondary antibodies (**B**). Immunoblots of extracts show the level of proteins in each condition. (**C–F**) Pull-down assays: HEK293 cells were transfected with Myc-Cortactin (**C–E**) or various deletion mutants of Myc-Cortactin (**F**) (ΔABR6, ΔABR5-6, ΔABR4-6, ΔABR3-6, ΔABR, ΔABR/NTA or ΔSH3, described in the schematic representation of Cortactin, bottom panel). NTA: N-Terminal acidic domain; ABR: actin binding repeat; Helix: helical domain; SH3: Src-homology three domain. Lysates were subjected to pull-down assays using GST, GST-p27 or GST-p27CK- (**C**), or GST, GST-p27, GST-p27 N_T (1-87) and GST-p27 C_T (88-198) (**D**), or GST, GST-p27CK-, GST-p27CK- (1-197) and GST-p27CK- (1-190) (**E**) or GST and GST-p27 (**F**). The amounts of Myc-Cortactin bound to the beads and of transfected protein present in the extracts were detected by immunoblot using mouse anti c-Myc (9E10) antibodies. The amounts of GST or GST p27 and mutants used in the assays were visualized by Coomassie staining of the gels. (**A–F**) All panels show representative results of at least three independent experiments.

To confirm the involvement of p27 in regulating invadopodia number and proteolytic activity, we retrovirally infected p27−/− E6 MEFs with either empty vector, wild-type (WT) p27, p27CK- or a p27CK- 1–190 truncation mutant (*Besson et al., 2004a*; *Serres et al., 2012*) that cannot interact with Cortactin (*Figure 1E*). Expression levels of p27 in these infected cells were determined by immunoblot (*Figure 3E*). Quantification of the number of cells forming invadopodia and of the area of gelatin degraded per cell indicated that expression of WT p27 and p27CK- significantly decreased both the number of p27−/− cells forming invadopodia and their capacity to degrade gelatin, while the p27CK- 1–190 mutant had no effect (*Figure 3F and G*). Thus, our data suggests that p27 limits invadopodia formation and that the domain mediating its interaction with Cortactin is required for this function.

The finding that p27 knockout cells more frequently form invadopodia and exhibit increased ECM degradation activity was surprising given the previous reports that p27 promotes migration and invasion (*Denicourt et al., 2007*; *Godin et al., 2012*; *Nguyen et al., 2006*; *Papakonstanti et al., 2007*; *Gui et al., 2014*; *Wu et al., 2006*; *See et al., 2010*; *Larrea et al., 2009*; *Jin et al., 2013*; *Zhao et al., 2015*; *Besson et al., 2004b*). We compared the motility of p27+/+, p27−/− and p27CK-/CK- E6 MEFs in 2D scratch wound assays and p27−/− cells had a migration defect (*Figure 4A and B*), in agreement with our previous findings (*Besson et al., 2004b*). We next measured the capacity of these MEFs to invade through a layer of Collagen I in transwell inserts. Similar to 2D migration, 3D invasion was reduced in p27−/− MEFs compared to either WT p27 or p27CK-expressing cells (*Figure 4C and D*), consistent with previous reports (*Denicourt et al., 2007*; *Gui et al., 2014*; *Wu et al., 2006*; *See et al., 2010*; *Jin et al., 2013*; *Zhao et al., 2015*). To confirm the involvement of p27 in regulating invasion, p27−/− E6 MEFs retrovirally infected with either empty vector, p27CK- or p27CK- 1–190 (*Figure 4E*, left panel) were subjected to transwell invasion assays. While p27CK- restored invasion of p27−/− cells, the p27CK- 1–190 mutant had no effect (*Figure 4E*, right panel). Taken together our results indicate that although p27 limits the number of invadopodia in MEFs, it also promotes cellular invasion through ECM. On the other hand, while p27-null cells more frequently form invadopodia and exhibit an increased capacity to degrade ECM, their ability to invade through matrix was significantly impaired.

p27 promotes the interaction of Cortactin with PAK1

Interestingly, a similar, seemingly paradoxical finding was recently reported, in which inhibition of Rac1, Trio or PAK1 with siRNAs caused a dramatic increase in invadopodia lifetime and in their capacity to degrade matrix, but this was accompanied by a sharp decrease in cell invasion (*Moshfegh et al., 2014*). In this study, activation of the Trio/Rac1/PAK1 pathway induced a putative PAK1-mediated phosphorylation of Cortactin and invadopodia disassembly, as expression of a S113A Cortactin mutant blocked this pathway (*Moshfegh et al., 2014*). In this study, altering the dynamics of invadopodia turnover inhibited invasion (*Moshfegh et al., 2014*).

To find out whether p27-null cells more frequently form invadopodia than p27+/+ cells (*Figure 3A and B*) due to an increase in their lifetime, we infected p27+/+ and p27−/− MEFs with Tks5-GFP to visualize invadopodia in live cells. Videomicroscopy analyses revealed that while invadopodia lifetime was on average 16.7 min in p27+/+ cells, their mean duration was 65.9 min in p27−/− cells (*Figure 5A*). Thus, invadopodia appear more stable in cells lacking p27.
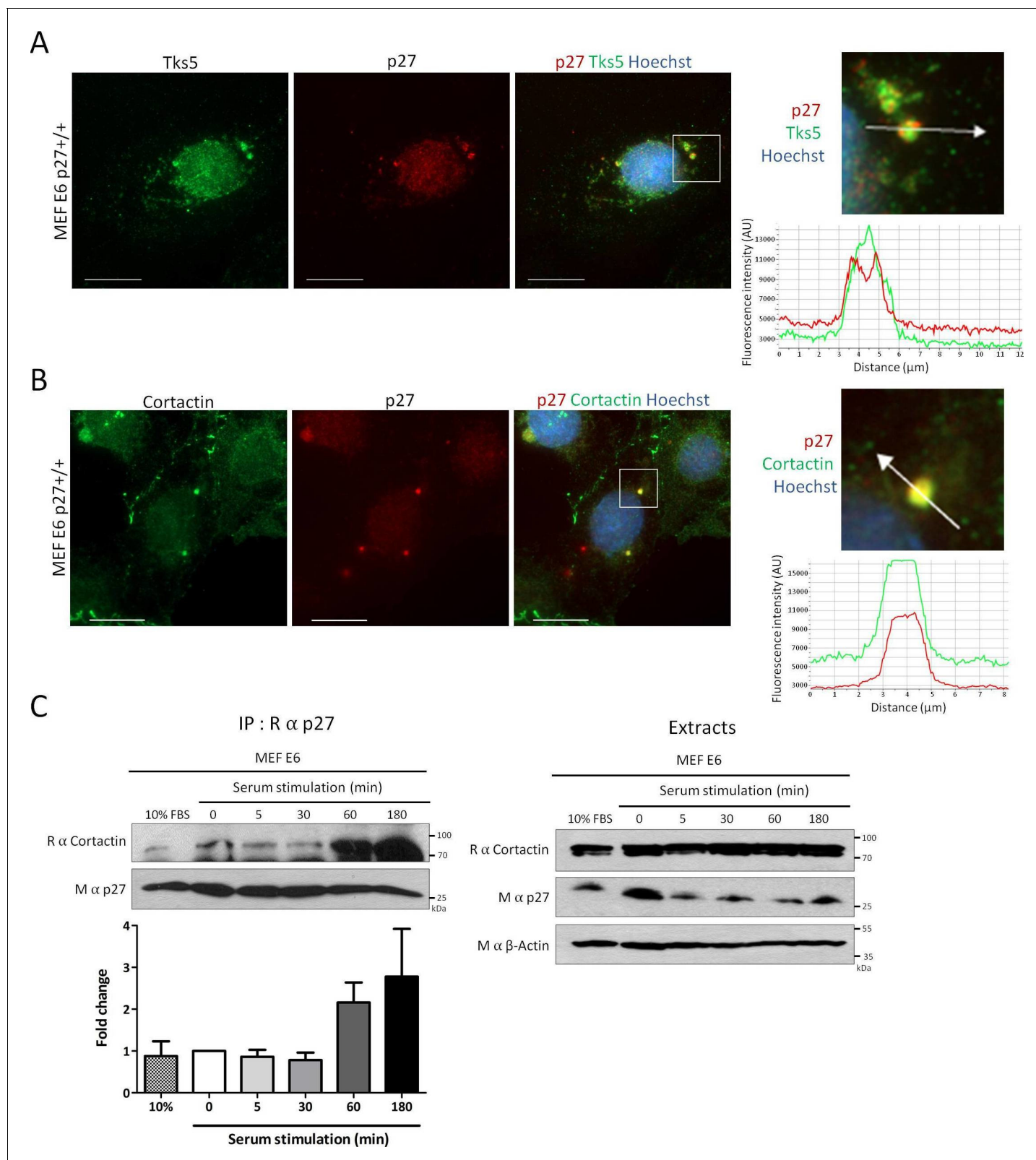
Figure 2. p27 colocalizes with Cortactin in invadopodia. (**A–B**) p27+/+ MEFs were seeded on gelatin-coated coverslips for 24 hr. Cells were permeabilized with digitonin prior to fixation. Cells were labeled with mouse anti p27 (SX53G8.5) in red (**A–B**) and rabbit anti-Tks5 (M-300) (**A**) or rabbit anti-Cortactin (H-191) (**B**) in green. Images were acquired using a 60x objective and images displayed are cropped areas. Graphs displaying the fluorescence intensity (arbitrary unit) under the arrows in the enlarged panels were generated with the NIS Element software. Scale bars: 20 μm. (**C**) p27

Figure 2 continued on next page

Figure 2 continued

+/+ E6 MEFs were starved overnight in DMEM-0.1% FCS and then stimulated with growth medium for the indicated times. Cell lysates were subjected to immunoprecipitation using rabbit anti-p27 (C–19). Immunoprecipitated proteins and corresponding cell extracts were immunoblotted with rabbit anti-Cortactin (H–191) and mouse anti-p27 (F–8) antibodies. β-actin was used as loading control. The graph represents the mean fold change in amounts of Cortactin co-precipitated with p27 in each condition compared to time zero from five independent experiments. These differences were not statistically significant.

The following source data and figure supplements are available for figure 2:

Source data 1. Quantification of co-immunoprecipitation between p27 and Cortactin in MEF E6 (*Figure 2C*) and HeLa cells (*Figure 2—figure supplement 2*).
Source data 2. Statistical analyses for *Figure 2C* and *Figure 2—figure supplement 2*.
Figure supplement 1. p27 colocalizes with Cortactin and Tks5 in different tumor cell lines.
Figure supplement 2. p27/Cortactin interaction in HeLa cells after EGF stimulation.

To determine whether p27 affects invadopodia formation through the regulation of Cortactin, we tested if binding of p27 to Cortactin regulated the interaction of Cortactin with some of its partners. p27 overexpression in Hela cells had no effect on the interaction of Cortactin with c-Src, ERK1 or Arp2 (*Figure 5—figure supplement 1*) (*Kirkbride et al., 2011*). Also, Cortactin acetylation levels did not change when p27 was overexpressed (*Figure 5—figure supplement 1*), suggesting that p27 did not affect the interaction of Cortactin with acetyltransferases such as p300, Tip60 and ATAT1 or the deacetylases HDAC6 and Sirt1 (*Sun et al., 2015*; *Zhang et al., 2007, 2009*; *Castro-Castro et al., 2012*). In contrast, the presence of p27 increased the amount of Cortactin co-immuno-precipitated with PAK1 in Hela cells (*Figure 5B*). Conversely, in MEFs lacking p27, the amount of Cortactin co-precipitated with PAK1 was sharply decreased compared to p27+/+ cells, despite the fact that PAK1 levels were elevated in p27−/− cells (*Figure 5C*). Monitoring the kinetics of association of PAK1 with Cortactin in MEFs revealed that some PAK1 is already associated with Cortactin in serum starved cells, consistent with a previous report (*Vidal et al., 2002*) and progressively increase after serum stimulation, reaching a maximal level after 3 hr (*Figure 5D and E*); mirroring the kinetics of association of p27 with Cortactin (*Figure 2C* and *Figure 2—figure supplement 2*). These results suggest that p27 binding to Cortactin promotes the association of PAK1 with Cortactin. Immunos-taining of p27+/+ MEFs showed a colocalization of PAK1 and p27 at structures resembling invado-podia (*Figure 5F*). However, despite repeated attempts on both endogenous and overexpressed proteins, we were unable to obtain evidence supporting an interaction between p27 and PAK1 (data not shown).

p27 regulates invadopodia formation via the Rac1/PAK1/phospho-Cortactin pathway

p27 promotes the interaction of PAK1 with Cortactin (*Figure 5A–D*), which in turn may promote invadopodia disassembly by phosphorylating Cortactin on Ser113 (*Moshfegh et al., 2014*). To test whether PAK1 activity is responsible for the low number of invadopodia observed in p27+/+ MEFs, we monitored the effect of either silencing PAK1 with siRNA or of the PAK1-3 specific inhibitors FRAX597 (*Licciulli et al., 2013*), FRAX1036 (*Ong et al., 2015*) and G-5555 (*Ndubaku et al., 2015*) on invadopodia formation and activity. While PAK1 silencing or the PAK1-3 inhibitors dramatically increased both the number of cells forming invadopodia and the area of matrix degraded per cell in p27+/+ MEFs, as reported previously (*Moshfegh et al., 2014*), it had no effect in p27−/− cells (*Figure 6A–B,D–F*, and *Figure 6—figure supplement 1A and B*). PAK1 silencing was verified by immunoblot for PAK1 in Control or PAK1 siRNA treated cells (*Figure 6C*). The efficacy of FRAX597, FRAX1036 and G-5555 in inhibiting PAK1 was evaluated by immunoblot on either vehicle or inhibitor treated cells using phospho-Ser144 PAK1/Ser141-PAK2 antibodies (*Figure 6G* and *Figure 6—figure supplement 1C*) (*Chong et al., 2001*). These results suggest that p27 acts downstream of PAK1 in
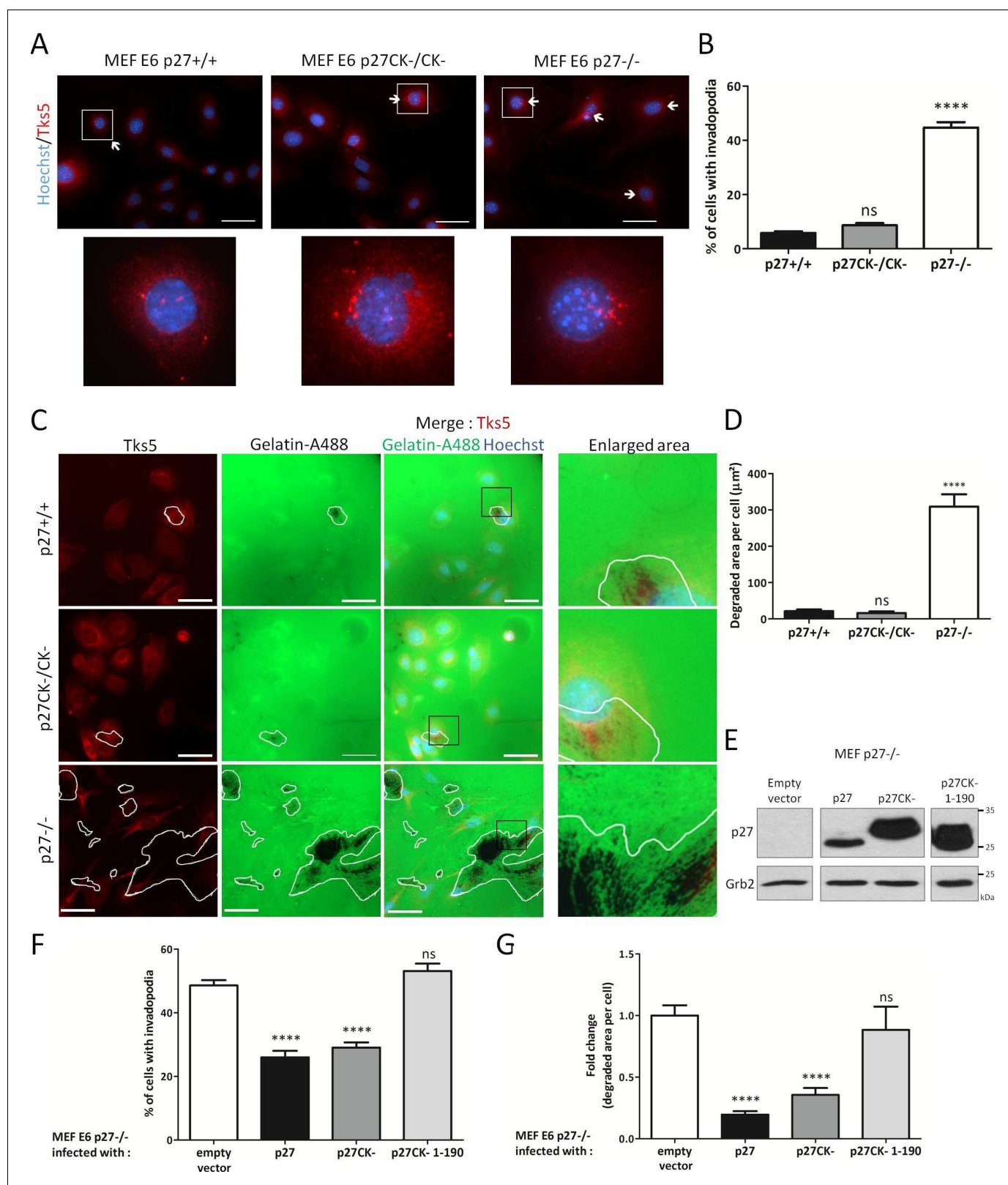
Figure 3. p27 regulates invadopodia formation and matrix degradation. (**A**) p27+/+, p27CK−/CK− and p27−/− immortalized MEFs were seeded on Oregon green-gelatin (gelatin-A488) for 16 hr. Cells were stained with rabbit anti-Tks5 (M-300) to visualize invadopodia. (**B**) The percentage of cells forming invadopodia was determined in a minimum of 15 fields, representing a minimum of 330 cells per genotype, for each experiment. The graph shows the mean of 3 independent experiments. (**C**) Cells were seeded as in (**A**). Tks5 staining shows invadopodia (red) and areas of degraded

Figure 3 continued on next page

Figure 3 continued

fluorescent gelatin indicate invadopodia activity (green). (D) The areas of degraded gelatin were measured in at least 15 fields per genotype in each experiment. The graph shows the mean of 3 independent experiments. (E–G) p27−/− E6 MEFs were infected with either empty vector or p27, p27CK− or p27CK− 1–190 vectors and then seeded on Gelatin-A488 for 48 hr. (E) p27 levels after retroviral infection were determined by immunoblot with rabbit anti-p27 (N-20) antibodies; Grb2 was used as loading control. (F–G) After Tks5 staining, invadopodia forming cells (F) were quantified as in B and area of degraded gelatin (G) as in D. Scale bars: 50 μm; 'ns' not significant; ****p<0.0001. In A and C, images were acquired using a 40x objective and images displayed are cropped areas.

The following source data and figure supplements are available for figure 3:

Source data 1. Quantification of cells with invadopodia (*Figure 3B*); quantification of degraded gelatin area per cell (*Figure 3C*); quantification of cells with invadopodia after p27 re-expression (*Figure 3F*) and quantification of degraded gelatin area per cell after p27 re-expression (*Figure 3G*).
Source data 2. Statistical analyses for *Figure 3B,C,F and G*.
Source data 3. Immunoblot scans of *Figure 3E*.
Figure supplement 1. p27+/+, p27CK−/CK− and p27−/− MEFs form functional invadopodia.
Figure supplement 2. p27 colocalizes with Tks5 at sites of gelatin degradation.

the regulation of invadopodia formation and activity, and that this pathway is impaired in p27−/− cells, possibly due to decreased PAK1/Cortactin interaction.

If p27 acts on the invadopodia disassembly pathway at the level of PAK1/Cortactin, one would not expect to see any difference in Rac1 activation levels in p27+/+ and p27−/− cells. This is what was observed by GTP-Rac1 pull-down assays (*Figure 7A*), in agreement with our previous observations (*Besson et al., 2004b*). Nevertheless, to further characterize how the Rac1/PAK1/Cortactin signaling pathway is affected in function of p27 status, we inhibited Rac1 itself using either Rac1 siRNAs (*Figure 7B–D*) or the Rac specific inhibitor NSC23766 (*Gao et al., 2004*) (*Figure 7E and F*). Rac1 silencing by siRNAs was verified by immunoblot for Rac1 (*Figure 7D*). When Rac1 was silenced or inhibited, more p27+/+ cells formed invadopodia and there was a dramatic increase in the area of matrix degraded (*Figure 7B,E and C,F*, respectively), as reported previously (*Moshfegh et al., 2014*). On the other hand, in p27−/− cells, Rac1 silencing or inhibition had no effect on invadopodia formation or gelatin degradation (*Figure 7B,E and C,F*, respectively); supporting the idea that p27 regulates invadopodia disassembly downstream of Rac1 and PAK1.

We previously reported that p27 binds RhoA and prevents its activation by its GEFs; consequently, cells lacking p27 have elevated RhoA activity (*Besson et al., 2004b*). Since RhoA plays a critical role in cell motility and the control of actin cytoskeleton dynamics, we determined whether RhoA was involved in p27-mediated regulation of invadopodia formation and function. Transfection of RhoA siRNAs in p27+/+ and p27−/− MEFs did not alter the proportion of cells forming invadopodia (*Figure 7—figure supplement 1A*) and only mildly increased the ability of both p27+/+ and p27−/− cells to degrade ECM, although this was not statistically significant (*Figure 7—figure supplement 1B*). RhoA siRNA efficacy was checked by immunoblot (*Figure 7—figure supplement 1C*). Furthermore, inhibition of the Rho effectors ROCK1/2 with a pharmacological inhibitor (Y27632) did not affect the ability of p27+/+ and p27−/− cells to invade through Collagen I in transwell invasion assays (*Figure 7—figure supplement 1D*). Thus, in MEFs, depletion of RhoA did not affect the ability of cells to form invadopodia and slightly increased invadopodia proteolytic activity independently of p27 status.

Evidence suggests that invadopodia disassembly by the Trio/Rac1/PAK1 signaling pathway is mediated by phosphorylation of Cortactin on Ser113 (*Webb et al., 2005*; *Moshfegh et al., 2014*). In the latter study, expression of an unphosphorylatable mutant of Cortactin (Cortactin S113A) increased both invadopodia lifetime and matrix degradation, as observed upon Rac1 or PAK1 silencing (*Moshfegh et al., 2014*). We retrovirally infected p27+/+ and p27−/− E6 MEFs with either empty vector, WT Cortactin, Cortactin S113A or the phosphomimetic mutant Cortactin S113D (*Figure 8A*) and monitored their effect on invadopodia formation and activity. In p27+/+ cells,
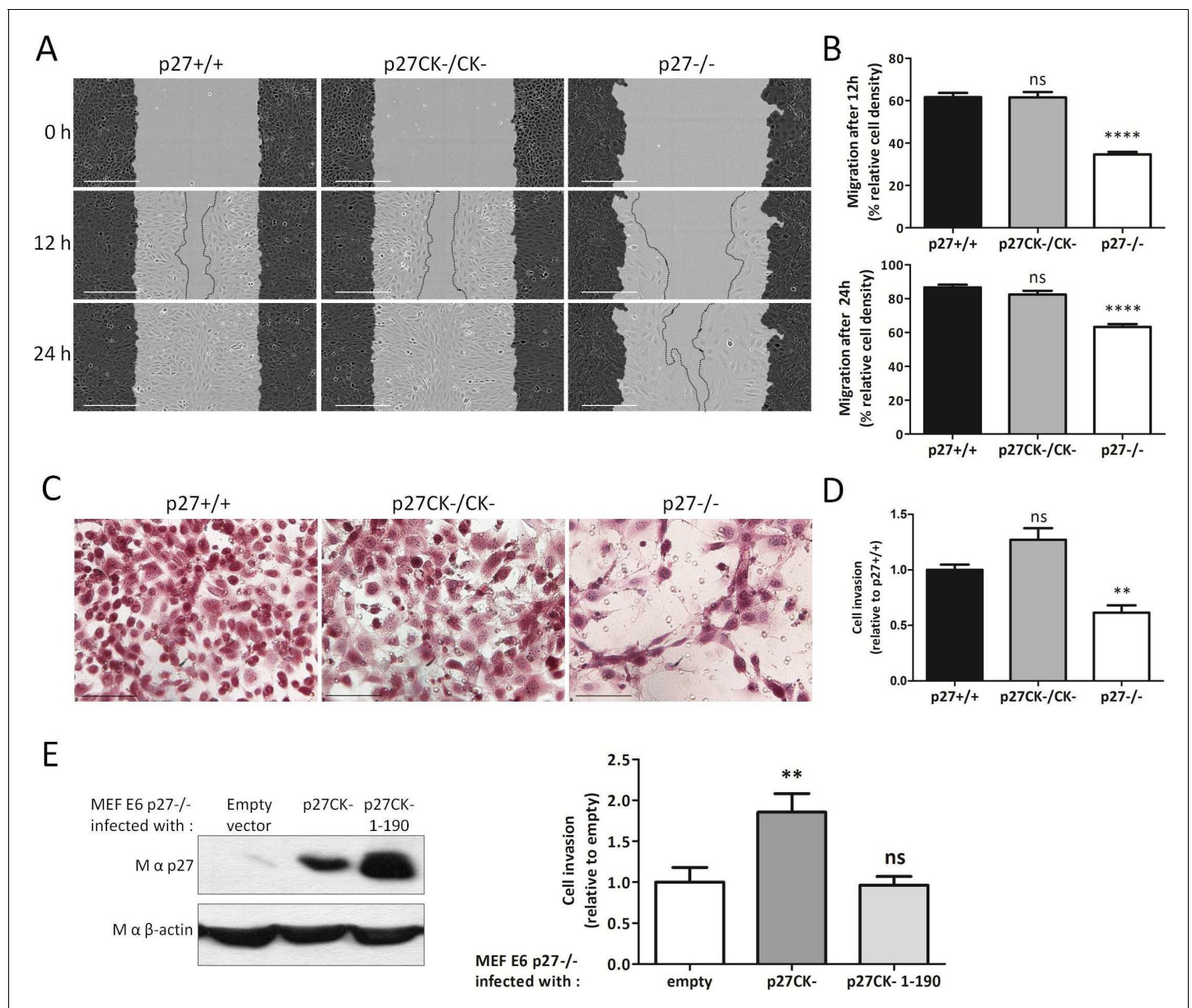
Figure 4. p27 promotes cell migration and invasion. (**A**) Representative images of scratch wound migration assays with p27+/+, p27CK−/CK− and p27−/− immortalized MEFs. Dark grey areas show the initial wound masks and dotted lines the migration fronts. Scale bars: 300 μm. (**B**) Mean cell migration at 12 hr and 24 hr post wounding for each genotype of five independent experiments. Percent of area in which the cells migrated, or wound closing (relative wound density) was calculated with the Incucyte software. 'ns': not significant; ****p<0.0001. (**C**) Representative images of p27+/+, p27CK−/CK− and p27−/− immortalized MEFs that invaded through a layer of Collagen I in transwell invasion assays and migrated to the bottom side of the transwell membrane after 48 hr. Scale bars: 100 μm. (**D**) The graph shows the mean number of cells that invaded through Collagen I quantified by XTT staining, expressed relative to p27+/+ cells, of three independent experiments. **p<0.01. (**E**) p27−/− E6 MEFs were infected with either empty vector, p27CK- or p27CK- 1–190 vectors and used in transwell invasion assays as in (**C–D**). p27 levels after retroviral infection were determined by immunoblot with mouse anti-p27 (SX53G8.5); β-actin was used as loading control. The graph shows the mean number of cells that invaded through Collagen I quantified by XTT staining, expressed relative to p27−/− cells, of four independent experiments.

DOI: 10.7554/eLife.22207.015

The following source data is available for figure 4:

Source data 1. quantification of relative wound density (*Figure 4B*); quantification of invasion (*Figure 4D*); and quantification of invasion rescue by p27 re-expression (*Figure 4E*).

DOI: 10.7554/eLife.22207.016

Source data 2. Statistical analyses for *Figure 4B,D and E*.

DOI: 10.7554/eLife.22207.017
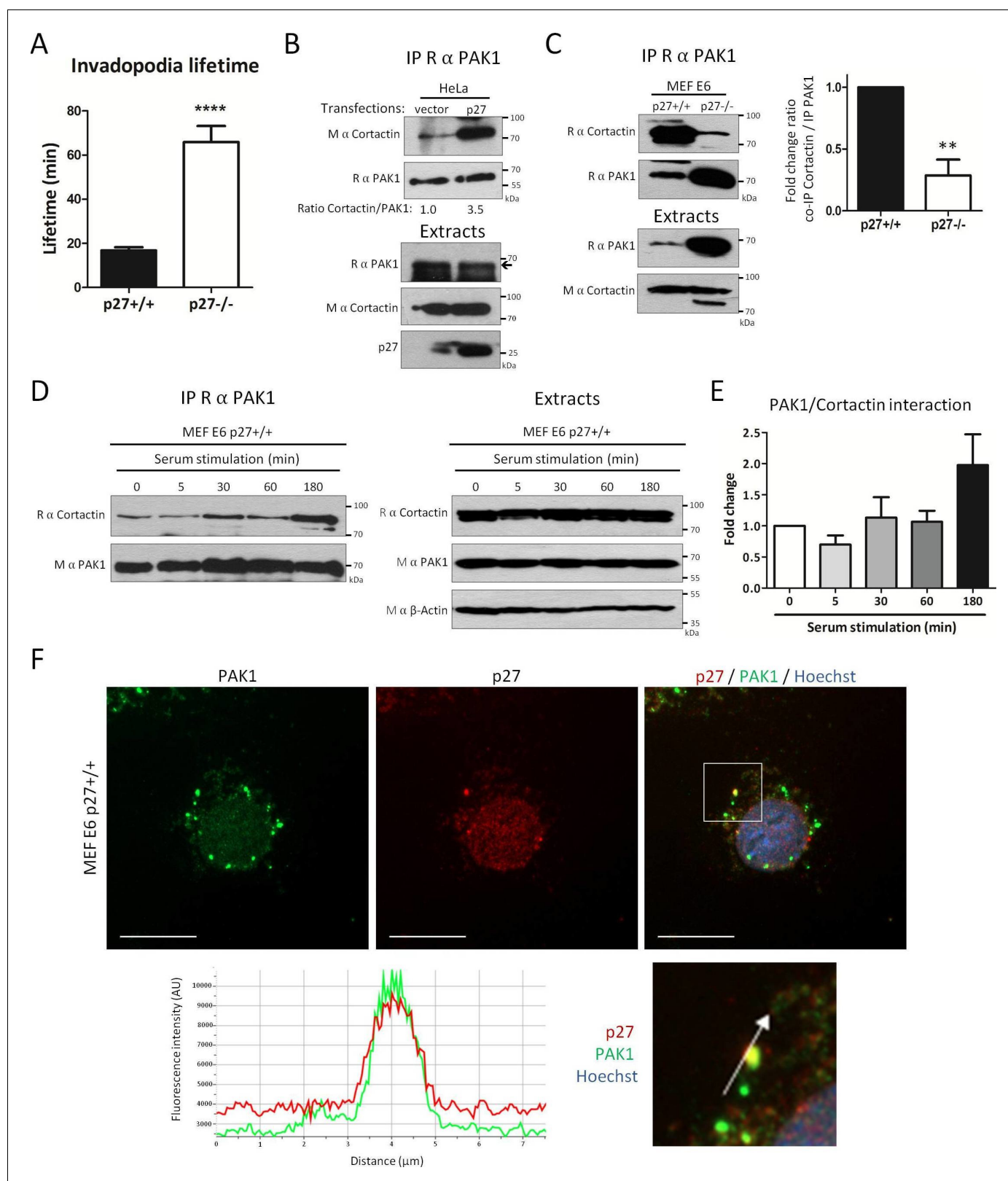
Figure 5. p27 promotes binding of Cortactin to PAK1. (**A**) Live p27+/+ and p27−/− immortalized MEFs expressing eGFP-Tks5 were imaged by videomicroscopy to measure invadopodia lifetime, using Tks5 as an invadopodia marker. The graph represents the average invadopodia lifetime of 20 invadopodia per genotype per experiment from three independent experiments. (**B–C**) Co-immunoprecipitations using rabbit anti-PAK1 (N-20) of HeLa cell lysates transfected with empty vector or p27 encoding vector (**B**) or p27+/+ and p27−/− E6 MEF lysates (**C**). Co-immunoprecipitated Cortactin was

Figure 5 continued on next page

Figure 5 continued

detected with mouse (**B**) or rabbit (**C**) anti-Cortactin antibodies. Immunoprecipitated PAK1 was visualized by reprobing the membranes with rabbit anti-PAK1 (N-20) and anti-Rabbit Ig light-chain secondary antibodies. Immunoblots of extracts show the level of proteins in each condition. In (**C**), the graph shows the mean fold change in the ratio of Cortactin to PAK1 co-immunoprecipitated, expressed relative to p27+/+ cells, in three independent experiments. **p<0.01. (**D**) p27+/+E6 MEFs were starved overnight in DMEM 0.1% FCS and then stimulated with growth medium for the indicated times. PAK1 was immunoprecipitated from cell lysates using rabbit anti-PAK1 (N-20). Immunoblots of immunoprecipitates (left panels) and extracts (right panels) were probed successively with rabbit anti-Cortactin (H-191) and anti-rabbit Ig light chain secondary antibodies and then with mouse anti-PAK1 (A6) antibodies. β-actin was used as loading control. (**E**) The graph shows the mean amount of Cortactin bound to PAK1 at each time-point from four independent experiments, normalized to time zero. These differences were not statistically significant. (**F**) p27+/+ MEFs were seeded on coverslips and permeabilized with digitonin prior to fixation. Cells were labeled with rabbit anti-PAK1 (N-20, green) and mouse anti p27 (SX53G8.5, red) antibodies. Images were acquired using a 60x objective and images displayed are cropped areas. The graph displaying the fluorescence intensity (arbitrary unit) under the arrow in the enlarged panel was generated with NIS Element software. Scale bars: 20 μm.

DOI: 10.7554/eLife.22207.018

The following source data and figure supplement are available for figure 5:

Source data 1. Quantification of invadopodia lifetime (*Figure 5A*); quantification of co-immunoprecipitation between Cortactin and PAK1 in MEFs (*Figure 5C*); and quantification of co-immunoprecipitation between Cortactin and PAK1 after serum stimulation (*Figure 5E*).

DOI: 10.7554/eLife.22207.019

Source data 2. Statistical analyses for *Figure 5A*.

DOI: 10.7554/eLife.22207.020

Source data 3. Statistical analyses for *Figure 5C*.

DOI: 10.7554/eLife.22207.021

Source data 4. Statistical analyses for *Figure 5E*.

DOI: 10.7554/eLife.22207.022

Figure supplement 1. p27 does not affect Cortactin acetylation or the recruitment of c-Src, Arp2 and ERK1 to Cortactin.

DOI: 10.7554/eLife.22207.023

Cortactin S113A increased the number of cells forming invadopodia, as observed previously (*Moshfegh et al., 2014*), while Cortactin S113D had no effect (*Figure 8B and D*). In contrast, Cortactin S113A had no effect in p27−/− cells, confirming that the Rac1/PAK1/Cortactin pathway is defective in absence of p27 and that p27 acts upstream of Cortactin. On the other hand, expression of Cortactin S113D in p27−/− cells decreased the number of invadopodia forming cells and the area of degraded gelatin (*Figure 8C and E*), indicating that mimicking Cortactin phosphorylation rescues the phenotype caused by the absence of p27.

Importantly, PAK3 was reported to phosphorylate Cortactin on several serine residues (S113, S150 and S282) within the actin binding repeats (*Webb et al., 2006*) suggesting that multiple phosphorylation events may synergize to regulate Cortactin function. To test this possibility, we generated triple alanine mutant (TA) (S113A/S150A/S282A) and triple aspartic acid mutant (TD) (S113D/S150D/S282D) of Cortactin and expressed these constructs in p27+/+ and p27−/− E6 MEFs (*Figure 8F*). Cortactin TA and TD mutants gave essentially similar results as the Cortactin S113A and S113D mutants, respectively (*Figure 8G–J*). Nevertheless, in p27+/+ MEFs, the Cortactin TA mutant was more potent than Cortactin S113A to promote invadopodia formation (13.5% p27+/+ cells forming invadopodia with Cortactin S113A versus 23.3% with Cortactin TA) and activity (6.17 fold increase in area of degraded gelatin with Cortactin S113A versus 10.02 fold with Cortactin TA) (*Figure 8B* versus *Figure 8G* and *Figure 8D* versus *Figure 8I*, respectively). This data suggests that Cortactin phosphorylation on S150 and/or S282 also contribute with S113 to control invadopodia disassembly. To further confirm that PAK-mediated phosphorylation events on Cortactin are involved in this pathway, we evaluated Cortactin phosphorylation levels in HEK 293 cells expressing Myc-tagged Cortactin treated or not with the PAK1-3 inhibitor FRAX597. In presence of FRAX597, there was a 36% decrease in P-Ser Cortactin level (*Figure 8—figure supplement 1A and B*). This mild reduction in P-Ser levels is consistent with Cortactin also being a substrate for other Ser/Thr kinases such as ERK, Akt and PKC. The contribution of S113, S150 and S282 phosphorylation in the P-Ser signal observed in Cortactin immunoprecipitates was estimated in HEK 293 cells expressing either wild-type Cortactin, Cortactin S113A or Cortactin TA. P-Ser levels were reduced in Cortactin S113A immunoprecipitations compared to WT Cortactin and further decreased in Cortactin TA immunoprecipitates, confirming that phosphorylation of these sites contribute to the Cortactin P-Ser signal in vivo (*Figure 8—figure supplement 1C*). Finally, to show that Cortactin was phosphorylated
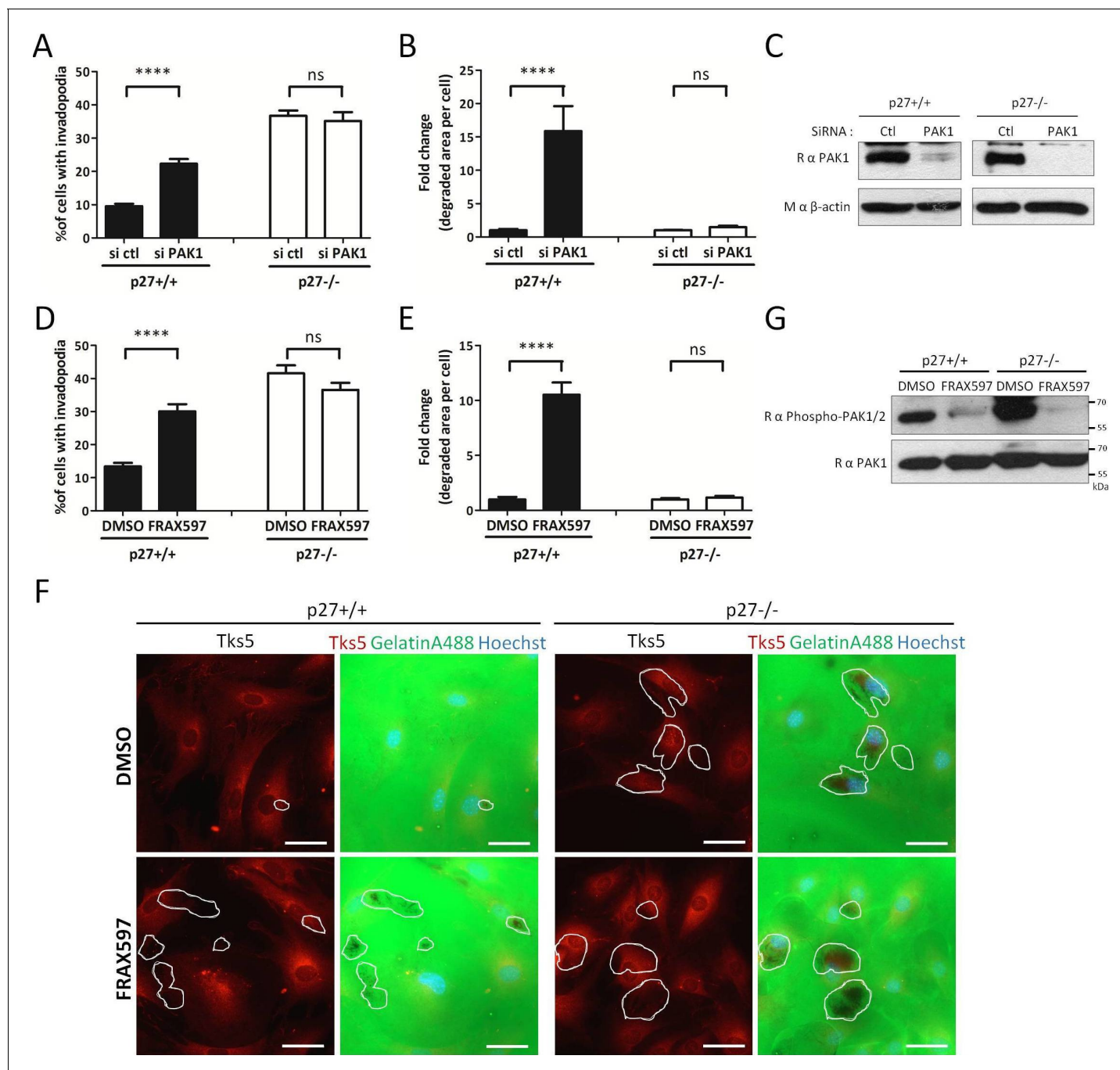
Figure 6. p27 regulates invadopodia formation downstream of PAK1. (**A–B**) p27+/+ and p27−/− E6 MEFs were seeded on gelatin-A488 and transfected with either control siRNAs or PAK1 siRNAs for 48 hr. Cells were stained with rabbit anti-Tks5 (M-300) to visualize invadopodia. At least ten fields per conditions were used to count cells forming invadopodia (**A**), representing a minimum of 212 cells per genotype for each experiment, or to measure the area of degraded gelatin, expressed in fold-change compared to vehicle treated conditions (**B**). (**C**) PAK1 siRNA efficacy at 48 hr was evaluated by immunoblot with rabbit anti-PAK1 (N-20) antibodies. β-actin was used as loading control. (**D–F**) p27+/+ and p27−/− E6 MEFs were seeded for 48 hr on gelatin-A488 and after 1 hr were treated with DMSO or 1 μM FRAX597, a PAK1-3 inhibitor. Quantification of cells forming invadopodia (**D**) and gelatin degradation (**E**) was performed as in (**A–B**), with a minimum of 215 cells counted per genotype per experiment. (**F**) Images were acquired using a 40x objective and images displayed are cropped areas. Scale bars: 50 μm. (**G**) FRAX597 inhibitor efficacy was evaluated by immunoblot with rabbit anti-phospho-Ser144-PAK1/phospho-Ser141-PAK2 and rabbit anti-PAK1 (N-20) antibodies. (**A–B**; **D–E**) The graphs show the mean of at least three independent experiments. ****p<0.0001.

DOI: 10.7554/eLife.22207.024

The following source data and figure supplement are available for figure 6:

Figure 6 continued on next page

in vivo on PAK-targeted sites (S113, S150 and/or S282), we performed mass spectrometry analyses on Cortactin. For this, HEK 293 cells were transfected with Myc-Cortactin alone or Myc-Cortactin and the myristoylated second SH3 domain of Nck1 (Myr-SH3-2), which was previously shown to activate PAK1 (*Lu et al., 1997*; *Lu and Mayer, 1999*). MS/MS analyses from Cortactin immunoprecipitates indicated that Cortactin was phosphorylated on S150 (*Figure 8—figure supplement 2*). This phosphorylation was detected only in samples from cells co-expressing Cortactin and Myr-SH3-2 suggesting that PAK1 activation is required for this event. Although no phosphorylation was detected on S113 or S282 in these experiments, phosphoproteome analyses from other studies have previously shown that Cortactin is phosphorylated in vivo on S113, S150 and/or S282: S113 phosphorylation was detected in prostate cancer cells (*Chen et al., 2010*), mouse brain (*Wiśniewski et al., 2010*) and breast cancers (*Mertins et al., 2016*). Phosphorylation on S150 was identified in mouse renal cells and human liver (*Bian et al., 2014*; *Rinschen et al., 2010*) and in the present study. S282 phosphorylation was detected in mitotic cells and breast cancers (*Mertins et al., 2016*; *Olsen et al., 2010*; *Klammer et al., 2012*). Phosphorylation on all three sites have been detected in ovarian and breast cancer xenogratfs (*Mertins et al., 2014*).

Altogether, our results indicate that p27 promotes invadopodia turnover and cell invasion via the Rac1/PAK1/Phospho-Cortactin pathway. In contrast, in absence of p27, this pathway is largely defective, resulting in increased invadopodia stability and elevated matrix degradation, but impaired invasion.

Discussion

Our results indicate that p27 regulates invadopodia formation and activity by binding to Cortactin, probably via the regulation of invadopodia turnover mediated by a signaling pathway recently characterized whereby signaling through Trio/Rac1/PAK1/Cortactin induces the disassembly of invadopodia (*Moshfegh et al., 2014*). The main finding presented here is that p27 directly controls cellular invasion by impinging on this pathway through the promotion of the Cortactin/PAK1 interaction and the phosphorylation of Cortactin on Ser113, S150 and/or S282 by PAK. Indeed, inhibiting the pathway upstream of Cortactin, either with Rac1 and PAK1 inhibitors or siRNAs converted the phenotype of p27+/+ cells to that of p27−/− cells. Conversely, artificially activating this pathway at the level of Cortactin using phosphomimetic mutants for the PAK-targeted sites efficiently rescued the phenotype of p27-null cells. All three phosphorylation sites on Cortactin appear to act synergistically as the phenotype caused by the triple mutants (Cortactin TA and TD) was more profound than that of mutating S113 alone. While mimicking the phosphorylation of Cortactin on PAK1-targeted sites clearly causes the disassembly of invadopodia (*Moshfegh et al., 2014*; *Webb et al., 2005*), the mechanism involved is still unclear but may be due to decreased affinity of Cortactin phosphorylated within its Actin-binding repeats for F-Actin, which may destabilize invadopodia (*Webb et al., 2006*).

Results from *Moshfegh et al. (2014)* and the present study show that inhibition of the Trio/Rac1/PAK1/Phospho-Cortactin pathway stabilizes invadopodia and is associated with a dramatic increase in proteolytic degradation of ECM. Surprisingly, this phenotype is accompanied by a sharp decrease in the ability of cells to invade through matrix in 3D invasion assays. Thus, it appears that the turnover of invadopodia rather than elevated ECM degradation is required for efficient invasion. Affecting the dynamics of invadopodia formation, maturation and disassembly is therefore detrimental to invasion, as observed here when this last step is inhibited by interfering with Rac1/PAK1 signaling or when p27 is absent. Interestingly, p27 also regulates cell migration in a similar manner by interfering
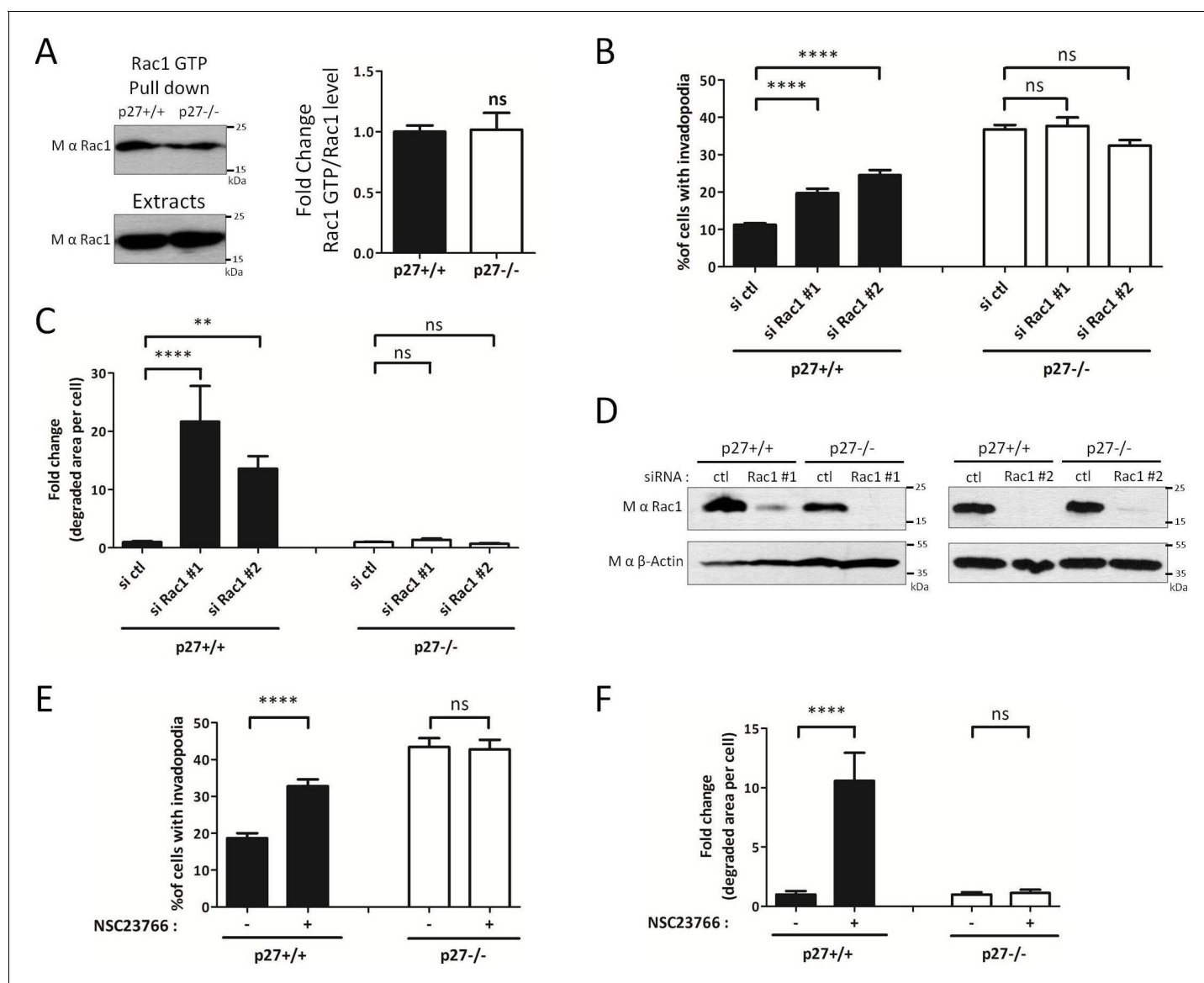
Figure 7. p27 regulates invadopodia formation downstream of Rac1. (A) Cells were seeded for 24 hr and Rac1-GTP levels measured by GTP pull-downs assays using GST-PAK1-CD beads. The amounts of Rac1-GTP bound to the beads and of total Rac1 in the extracts were detected by immunoblot with mouse anti-Rac1. The graph shows the mean ratio of GTP-Rac1/total Rac1 from six independent experiments. (B–D) Cells were transfected with control (ctl) or Rac1 #1 or #2 siRNAs for 3 days. Cells were then seeded on Gelatin-A488 for 48 hr and for monitoring siRNA efficiency. Cells were stained with rabbit anti-Tks5 (M-300) to visualize invadopodia. At least ten fields per condition were used to count cells forming invadopodia, representing a minimum of 197 cells per genotype for each experiment (B) or to measure the area of degraded gelatin, expressed in fold-change compared to control siRNA treated conditions (C). (D) Rac1 silencing was evaluated by immunoblot with mouse anti-Rac1. β-actin was used as loading control. (E–F) Cells were processed as described in *Figure 6D and E* except that the Rac1 inhibitor NSC23766 at 100 µM was used instead of FRAX597. A minimum of 153 cells were counted per genotype for each experiment. (B–C; E–F) The graphs show the mean of at least three independent experiments. ****p<0.0001; **p<0.01.

The following source data and figure supplement are available for figure 7:

Source data 1. Quantification of Rac1 GTP/Rac1 levels (*Figure 7A*); quantification of invadopodia forming cells (*Figure 7B*) and degraded gelatin area (*Figure 7C*) after silencing of Rac1; quantification of invadopodia forming cells (*Figure 7E*) and degraded gelatin area (*Figure 7F*) after NSC23766 treatment; quantification of invadopodia forming cells (*Figure 7—figure supplement 1A*) and degraded gelatin area (*Figure 7—figure supplement 1B*) after RhoA silencing; and quantification of invasion after Y27632 treatment (*Figure 7—figure supplement 1D*).

Source data 2. Statistical analyses for *Figure 7A,B,C,E,F*, and *Figure 7—figure supplement 1A,B and D*.

Figure 7 continued on next page

Figure 7 continued

Figure supplement 1. RhoA regulation by p27 is not involved in invadopodia formation.

with RhoA activation by its GEFs (*Besson et al., 2004a*, *2004b*). In absence of p27, cells accumulate actins stress fibers and focal adhesions and exhibit a migration defect due to an imbalance in the dynamic cycles of RhoA activation and inactivation (and concomitant Rac1 inactivation and activation) required for F-actin turnover, focal adhesion disassembly and efficient migration (*Besson et al., 2004a*, *2004b*; *Ren et al., 2000*; *Arthur and Burridge, 2001*; *Cox et al., 2001*; *Sahai et al., 2001*; *Vial et al., 2003*). Migration and invasion are two intimately linked processes (*Friedl and Wolf, 2003*; *Petrie and Yamada, 2016*). It is quite remarkable that p27 appears to regulate both of these processes, although by distinct mechanisms. Indeed, p27 binds to RhoA and Cortactin via the same domain located within the last 8 aa of the protein (*Figure 1E*) (*Larrea et al., 2009*; *Godin et al., 2012*), but while RhoA preferentially binds p27 phosphorylated on T198 (*Larrea et al., 2009*), the interaction of p27 with Cortactin did not require the presence of T198 (*Figure 1E*), suggesting that different pools of the protein are involved in their regulation. In addition, the regulation of invadopodia by p27 did not appear to involve RhoA, as RhoA silencing affected both p27−/− and p27+/+ cells in a similar manner (*Figure 7—figure supplement 1*). p27 also regulates invasion by promoting EMT, notably through JAK2/STAT3 signaling and induction of the transcription factor Twist (*Zhao et al., 2015*).

We found that p27 binds to Cortactin on its actin-binding repeats and this interaction promoted the association of Cortactin with PAK1. Since we were unable to detect an interaction between p27 and PAK1 using either endogenous or overexpressed proteins, it remains unknown how p27 promotes the PAK1/Cortactin interaction. Evidence suggest that Cortactin is an intrinsically disordered protein (IDP), especially its actin-binding repeats (*Shvetsov et al., 2009*) and p27 is a well-known IDP (*Galea et al., 2008*; *Lacy et al., 2004*; *Ou et al., 2012*). Since these proteins typically fold upon binding to their partners, an attractive possibility is that p27 binding causes a conformation change in Cortactin that would favor its interaction with PAK1.

p27 is a cyclin-CDK inhibitor and although p27 regulates migration and invasion in a CDK-independent manner (*Besson et al., 2004b*; *Larrea et al., 2009*; *Zhao et al., 2015*; *Gui et al., 2014*), there is evidence to suggest that some cell cycle independent roles of CDKs and cyclins may be mediated via CDK inhibitors such as p27 (*Hydbring et al., 2016*). For instance, the regulation of cell migration by Cyclin D1 requires p27 (*Li et al., 2006*) and the role of CDK5 in promoting neuronal progenitor migration in vivo is mediated via the phosphorylation of p27 on Ser10 which regulates the RhoA/ROCK/LIMK/Cofilin pathway (*Nguyen et al., 2006*; *Kawauchi et al., 2006*). Interestingly, CDK5 was recently found to play an important role in invadopodia formation and cancer cell invasion, and CDK5 inhibition blocked both these processes (*Quintavalle et al., 2011*; *Bisht et al., 2015*). CDK5 phosphorylated Caldesmon, causing its degradation by the proteasome and promoting invadopodia formation and invasion (*Quintavalle et al., 2011*). Since p27 is a poor inhibitor of CDK5 complexes (*Lacy et al., 2005*; *Lee et al., 1996*), it would be interesting to test whether this role of CDK5 may involve p27. Indeed, an attractive hypothesis is that p27 could simultaneously interact with CDK5 complexes, via its N-terminal cyclin-CDK binding domain, and with Cortactin via its C-terminus, thereby recruiting CDK5 in proximity to Caldesmon bound to Cortactin and allowing Caldesmon phosphorylation.

Our study further defines the complex role played by p27 in the regulation of cytoskeletal dynamics, migration, EMT and invasion and provides another element to explain why the *Cdkn1b* gene is rarely mutated in cancer (*Chu et al., 2008*; *Besson et al., 2008*; *Kandoth et al., 2013*). Indeed, p27 is either downregulated, mostly via increased proteasomal degradation, or excluded from the nuclei of cancer cells. Given that upon cytoplasmic relocalization, p27 promotes both migration and invasion and may serve to coordinately regulate these processes, it appears likely that this feature may be selected for during tumor progression and could participate in the acquisition of a metastatic behavior by cancer cells.
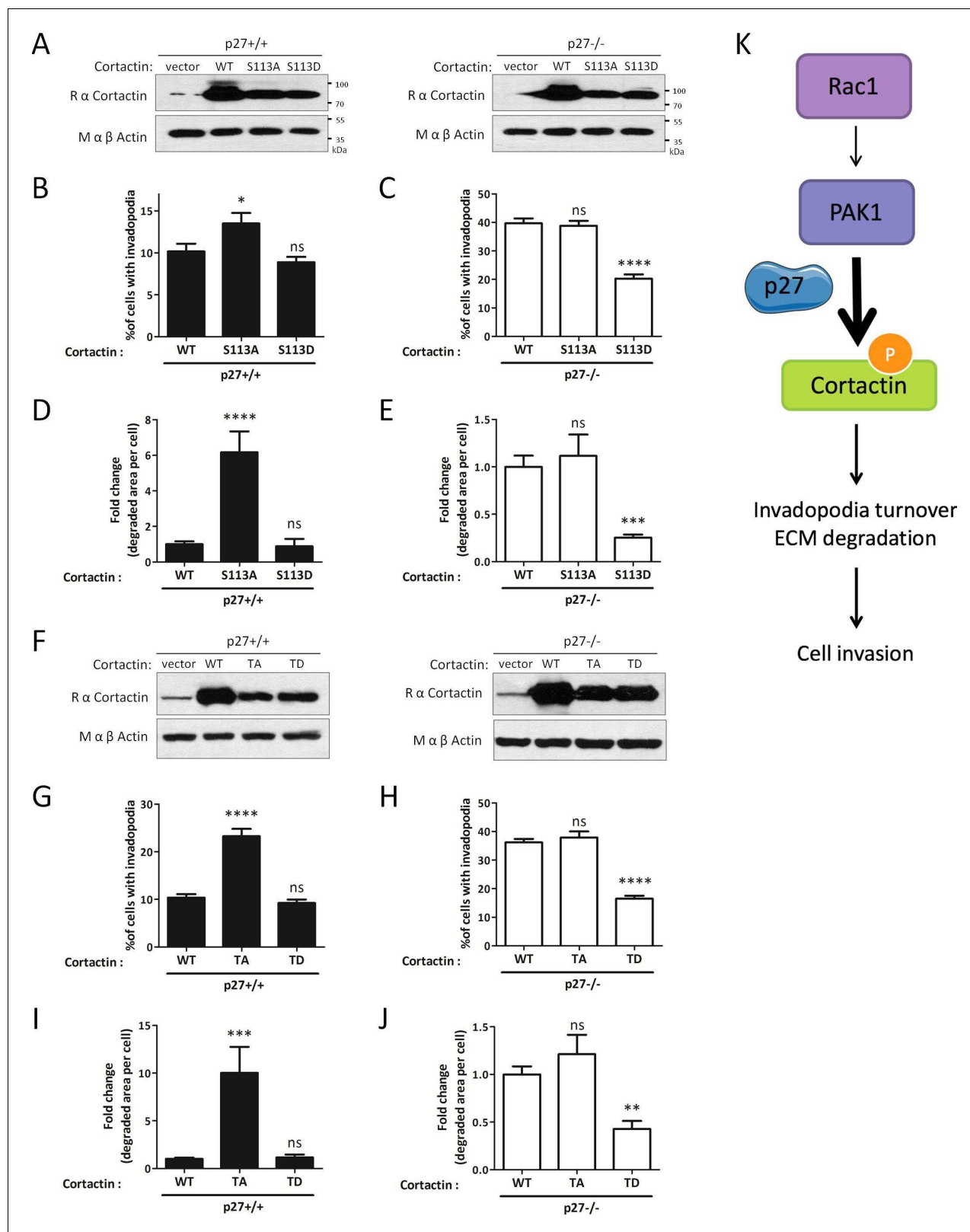
Figure 8. Mimicking phosphorylation of Cortactin restores invadopodia dynamics in p27−/− cells. (A–E) p27−/− E6 MEFs were infected with empty vector or with vectors encoding wild type Cortactin (WT), S113A-Cortactin (S113A) or S113D-Cortactin (S113D). (A) Cortactin levels after retroviral infection were determined by immunoblot with rabbit anti-Cortactin (H-191) antibodies. β-actin was used as loading control. (B–E) Cells were seeded on gelatin-A488 for 48 hr. After Tks5 staining, cells forming invadopodia (B–C), or the area of degraded gelatin, expressed in fold-change compared to

Figure 8 continued on next page

Figure 8 continued

WT Cortactin transfected cells (**D–E**), were quantified in at least ten fields per condition in each experiment, representing a minimum of 179 cells per genotype. The graphs show the means of at least three independent experiments. (**F–J**) p27−/− E6 MEFs were infected with empty vector or with vectors encoding WT Cortactin, Cortactin TA (S113A/S150A/S282A) or Cortactin TD (S113D/S150D/S282D). (**J**) Cortactin levels after retroviral infection were determined as in (**A**). (**G–J**) Cells were processed as in (**B–E**) to quantify cells forming invadopodia (**G–H**), or the area of degraded gelatin (**I–J**), with a minimum of 222 cells counted per genotype per experiment. The graphs show the means of 3 independent experiments. (**K**) Schematic representation of the Rac1/PAK1/phospho-Cortactin pathway involved in invadopodia turnover and matrix degradation and its proposed regulation by p27. ****$p < 0.0001$; ***$p < 0.001$; **$p < 0.01$; *$p < 0.05$.

DOI: 10.7554/eLife.22207.032

The following source data and figure supplements are available for figure 8:

Source data 1. Quantification of cells forming invadopodia (*Figure 8B–C*) and degraded gelatin area (*Figure 8D–E*) after infection with S113 phospho-mutants of Cortactin; quantification of cells forming invadopodia (*Figure 8G–H*) and degraded gelatin area (*Figure 8I–J*) after infection with triple phospho-mutants of Cortactin; quantification of P-Ser Cortactin/Cortactin ratio (*Figure 8—figure supplement 1B*).
DOI: 10.7554/eLife.22207.033

Source data 2. Statistical analyses for *Figure 8*.
DOI: 10.7554/eLife.22207.034

Source data 3. Statistical analyses for *Figure 8—figure supplement 1B*.
DOI: 10.7554/eLife.22207.035

Source data 4. Mascot search results for Cortactin for *Figure 8—figure supplement 2*.
DOI: 10.7554/eLife.22207.036

Figure supplement 1. Cortactin is phosphorylated on S113/S150 and/or S282 in vivo.
DOI: 10.7554/eLife.22207.037

Figure supplement 2. Cortactin is phosphorylated on S150 in vivo upon PAK activation.
DOI: 10.7554/eLife.22207.038

Materials and methods

Antibodies, reagents and plasmids

Mouse anti c-Myc (9E10, sc-40, RRID:AB_627268), p27 (F8, sc-1641, RRID:AB_628074), p27 (SX53G8.5, sc-53871, RRID:AB_785029), αPAK (A6, sc-166887, RRID:AB_10609226), RhoA (26C4, sc-418, RRID:AB_628218) and rabbit anti p27 (C19, sc-528, RRID:AB_632129), Myc (A14, sc-789, RRID:AB_631274), Cortactin (H191, sc-11408, RRID:AB_2088281), Tks5 (M-300, sc-30122, RRID:AB_2254551), αPAK (N-20, sc-882, RRID:AB_672249), Arp2 (H-84, sc-15389, RRID:AB_2221848), c-Src (SRC2, sc-18, RRID:AB_631324) and ERK1 (K-23, sc-94, RRID:AB_2140110) antibodies were purchased from Santa Cruz Biotechnology. Mouse anti p27 (610242), Grb2 (610112, RRID:AB_397518), Cortactin (610050, RRID:AB_397462), phopsho-Ser (612547, RRID:AB_399842) and Rac1 (610650, RRID:AB_397977) antibodies were purchased from BD-Transduction Laboratories. Mouse anti β-actin (A2228, RRID:AB_476697) antibody was purchased from Sigma-Aldrich. Rabbit anti phospho-Ser144-PAK1/phospho-Ser141-PAK2 (#2606, RRID:AB_2299279) antibody was purchased from Cell Signalling Technology. Rabbit anti acetyl-Cortactin (#09–881, RRID:AB_10584980) antibody was purchased from Millipore. Secondary antibodies against whole Ig or Ig light-chain conjugated to horse-radish peroxydase or Cyanine-2–3 and −5 were from Jackson ImmunoResearch (RRID:AB_10015282, RRID:AB_2340612, RRID:AB_2307443, RRID:AB_2340607, RRID:AB_2340770, RRID:AB_2340826, RRID:AB_2340813, RRID:AB_2340819, RRID:AB_2339149, RRID:AB_2338512).

siRNA control (D-001810-10-05), ON-TARGETplus Mouse Rac1 (19353) siRNA - SMARTpool (L041170000005) (#2) and ON-TARGETplus Mouse PAK1 (18479) siRNA - SMARTpool (L048101000005) were from Dharmacon. mRac1 siRNA (#1) (sc-36352), mRhoA siRNA (#1) (sc-29471) and mRhoA siRNA (#2) (sc-36414) were purchased from Santa Cruz Biotechnologies.

FRAX597 and Y-27632 were purchased from Selleckchem. NSC23766 was purchased from Tocris Biosciences. FRAX1036 and G-5555 were purchased from MedChemExpress.

p27 constructs and p27 point mutants and deletion mutants in pCS2+, pGEX4T1 (Pharmacia), pET16b (Novagen), pcDNA3.1 Hygro (Invitrogen) or pQCXIP (Clontech) were described previously (*Besson et al., 2004b*; *Serres et al., 2012*). The Myc-tagged full-length and deletion mutants of mouse Cortactin (WT, ΔABR6, ΔABR5-6, ΔABR4-6, ΔABR3-6, ΔABR, ΔABR/NTA and ΔSH3) in pME18S vector were described previously (*Katsube et al., 2004*). Full length human Cortactin was cloned by RT-PCR from IMR90 mRNA and inserted into the pcDNA3.1 Hygro Myc vector. Full-length

mouse Cortactin, Cortactin S113A and Cortactin S113D were kindly provided by Dr. Alan Mak (Queen's University, Kingston, Canada) (Webb et al., 2006) and subcloned into pQCXIP. Cortactin TA (S113A, S150A and S282A) and TD (S113D, S150D and S282D) were generated by site-directed mutagenesis from the pQCXIP-Cortactin-S113A and pQCXIP-Cortactin-S113D vectors, respectively. GFP-Tks5, kindly provided by Dr. Frederic Saltel (INSERM UMR1053, Bordeaux), was subcloned into the pQCXIP vector. pCMV6-Myc-hPAK1 was kindly provided by Dr Jonathan Chernoff (Fox Chase Cancer Center, Temple Health, Philadelphia; Addgene #12209). pGEX2TK-PAK-CD was kindly provided by Dr. John Collard (The Netherlands Cancer Institute, Amsterdam, The Netherlands). pEBB-Src-SH3-2 encoding the second SH3 domain of Nck1 fused to the myristoylation sequence of Src (myr-SH3-2) was a gift from Dr Bruce Mayer (University of Connecticut, Farmington). All plasmids used in this study were verified by sequencing.

Cell culture and transfections

Primary MEFs were prepared as described previously (Spector, 1997; Besson et al., 2004b) from p27+/+, p27CK−/CK− or p27−/− embryos. MEFs were immortalized by infection with retroviruses encoding the human papilloma virus E6 protein and hygromycin selection. HeLa (RRID:CVCL_0030), HEK 293 (RRID:CVCL_0045), A-375 (RRID:CVCL_0132) and A549 (RRID:CVCL_0023) cells were obtained from Cell Lines Services. These cells were authenticated by short tandem repeat profiling. All cells were routinely tested to be free of mycoplasma contamination by DAPI staining.

All cells were grown at 37°C and 5% CO_2 in DMEM (Sigma), 4.5 g/l glucose supplemented with 10% fetal calf serum, 0.1 mM nonessential amino acids and 2 µg /ml penicillin-streptomycin. When indicated, tissue culture vessels were coated with 0.2% gelatin from bovine skin (Sigma G1393) for 1 hr. MEFs were infected with different plasmids using retroviruses produced in Phoenix ecotropic cells transfected by the calcium phosphate method. HEK293 cells were also transfected by the calcium phosphate method for 24 hr. HeLa cells were transfected using JetPrime (Polyplus transfection) according to manufacturer's instructions. For siRNA transfections in MEF E6 cells, we used Interferin (Polyplus transfection) according to manufacturer's instructions.

Immunoprecipitation and GST pull-down

Cells were scraped and lysed in IP buffer containing 50 mM HEPES pH 7.5, 150 mM NaCl, 1 mM EDTA, 2.5 mM EGTA, 0.1% Tween20, 10% glycerol and 1% NP-40 complemented with 1 mM DTT, 10 mM β-glycerophosphate, 10 mM NaF, 10 mM sodium orthovanadate, 10 µg/ml Aprotinin, 10 µg/ml Bestatin, 10 µg/ml Leupeptin and 10 µg/ml Pepstatin A. After sonication for 10 s, cells extracts were centrifuged for 5 min at 12,500 g and supernatants were collected. Lysates (300 µg for MEF E6 and HeLa, 500 µg for HEK293) were incubated with 3 µg of indicated antibodies and 12 µl protein-A sepharose beads (IPA300, Repligen) (co-immunoprecipitation) or with recombinant GST proteins and glutathione sepharose beads (Pharmacia) (GST pull-down) at 4°C for 4 hr. Beads were then washed four times in lysis buffer and resuspended in 10 µl 4X sample buffer, boiled, and subjected to western blotting.

Rac1-GTP pull-down assay

Pull-down assays for Rac1 activity were performed as described previously (Besson et al., 2004b; Sander et al., 1998; Malliri et al., 2000). Briefly, E6 MEFs in 100 mm plates were washed with ice-cold PBS, scraped off the plates in 400 µl cell-lysis buffer (50 mM Tris-HCl at pH 7.4, 2 mM MgCl2, 1% NP-40, 10% glycerol, 100 mM NaCl, complemented with 1 mM dithiothreitol, 10 µg/ml leupeptin, 10 µg/ml aprotinin, and 10 µg/ml pepstatin-A) on ice. Lysates were centrifuged for 5 min at 14,000 rpm at 4°C. Three hundred µl of cleared lysates were incubated for 30 min at 4°C with 8 µl of GST–PAK-CD bound to glutathione-coupled Sepharose beads (at ~1 µg GST fusion protein per µl of beads). Bead pellets were washed three times with ice-cold cell lysis buffer, resuspended in 4X sample buffer, and subjected to SDS-PAGE as described below. Ten µl of cell lysates were used for protein loading.

Immunoblot

Cells were lysed in IP buffer as described above. Lysates and immunoprecipitates were mixed with 4X sample buffer and boiled. Proteins were resolved on 8–15% SDS-PAGE (depending on protein

size) and transferred to polyvinylidene difluoride membrane (Immobilon-P, Millipore). Membranes were blocked with PBS-T (PBS, 0.1% Tween-20), 5% non-fat dry milk and probed with indicated primary antibodies overnight at 4°C with gentle agitation. Membranes were washed three times in PBS-T then incubated with corresponding HRP-conjugated secondary antibody (1/10000) for 4 hr at room temperature. Bands were visualized using enhanced chemiluminescence detection reagents (Millipore, BioRad, Ozyme) and autoradiographic film (Blue Devil).

Gelatin degradation assay
Coverslips were cleaned overnight in 1 M HCl, washed four times in ddH$_2$O and then coated successively with 50 µg/ml Poly L-lysine, 0.5% glutaraldehyde, fluorescent gelatin (1:10 mix of gelatin from pig skin Oregon green 488 conjugate [G13186, Molecular Probes] and 0.2% gelatin from bovine skin [Sigma G1393]), and 5 mg/ml sodium borohydride. Between each coating, coverslips were washed three times with PBS. Coverslips were then sterilized with 70% ethanol and cells were seeded and incubated either overnight or 48 hr before fixation and staining.

Immunofluorescence
Cells were seeded on coverslips coated as described above with only non fluorescent gelatin and grown overnight. When indicated, cells were permeabilized with 20 µg/ml digitonin in PBS for 2 min before fixation. Cells were fixed with 2% PFA in PBS for 20 min at 37°C. For immunostaining, cells were permeabilized for 3 min with PBS 0.2% Triton X-100, rinsed three times in PBS and incubated for 20 min in blocking solution (PBS, 3% BSA, 0,05% Tween20 and 0,08% sodium azide) and with primary antibodies diluted in blocking solution for 1 hr. After three washes of 5 min in PBS, cells were incubated for 30 min at 37°C with Cy-2 Cy-3 or Cy-5 conjugated secondary antibodies at 1:500 dilutions. Coverslips were washed 3 times for 5 min in PBS with the first wash containing 0.1 µg/ml Hoechst H33342 and mounted on glass slides with gelvatol (20% glycerol (v/v), 10% polyvinyl alcohol (w/v), 70 mM Tris pH 8). Images were captured on a Nikon 90i Eclipse microscope using a DS-Qi2 HQ (Nikon) camera and the NIS Element software.

For live cell imaging, MEFs infected with pQCXIP-Tks5-GFP were seeded in gelatin-coated wells overnight and placed in a controlled atmosphere chamber (37°C and 5% CO$_2$) for imaging. Images were acquired every 2 min with a Zeiss Cell Observer microscope for 8 hr. Image analysis was performed with Image J/Fiji.

Migration assays
Cells were seeded in gelatin coated 96-well plates (Essen ImageLock, Essen Bioscience) at 80% confluence and incubated overnight to allow them to reach confluence. Cells were treated for 2 hr before wounding with 2 µg/ml mitomycin C (M4287, Sigma) to block cell proliferation and scratches were performed in the cell monolayer using the wound maker (Essen Bioscience). Cells were washed immediately three times with PBS and re-fed with growth medium. Cell migration was monitored with an Incucyte FLR Live-Cell imaging system equipped with a 20X objective (Essen Bioscience). Images were acquired every 3 hr for 48 hr. Migration was quantified by measuring the relative wound density of at least three biological replicates in each experiment, using the Incucyte software (Essen Bioscience) as recommended by the manufacturer.

Invasion assays
Fifty µl of 1 mg/ml of rat tail Collagen I (354236, Corning) solution were incubated for 1 hr at room temperature in 8 µm pores transwell inserts in 24-well plates (#353097, Corning) to allow gelling of collagen. The gel was hydrated with DMEM-50% FCS for 3 hr at 37°C. Cells were incubated for 3 hr with 2 µg/ml Mitomycin C, washed twice with DMEM 0.1% FCS, trypsinized, counted and 30,000 cells were seeded in the transwell upper chamber in 100 µl of DMEM 0.1% FCS, with 600 µl of DMEM 10% FCS in the bottom chamber. Plates were incubated for 48 hr at 37°C and 5% CO$_2$. At the end of the assay, the content of the top chamber was removed with a cotton swab and cells that invaded onto the bottom membrane of the transwell were quantified by XTT staining with 200 µg/ml XTT (Santa-Cruz Biotechnology, sc-258336) previously activated by adding 25 µM phenazine methosulfate (Sigma, P9625) in DMEM 10% FCS for 4 hr at 37°C. Absorbance was read at 450 nm.

Cells were then fixed for 5 min in 95% ethanol/5% acetic acid and stained overnight with hematoxylin to capture images of invaded cells.

Statistical analyses

Statistical analyses were performed using Graphpad Prism 6.0 software. Differences between groups were evaluated using 1-way ANOVA followed by Bonferroni test for multiple comparison and considered significant when $p<0.05$. Data are presented as mean ± SEM.

Mass spectrometry analyses

HEK293 cells were transfected either with human Myc-tagged Cortactin or Myc-Cortactin and Myr-SH3-2 (that activates PAK1) for 24 hr. Cortactin was immunoprecipitated from lysates from four 100 mm plates per IP using 12 µg per IP of Mouse anti-Myc 9E10 antibody. Samples were separated on 12% SDS-PAGE. Gel was stained with instant blue for 1 hr. Amounts of immunoprecipitated Cortactin was estimated to 4 ug for each IP by comparison with a BSA standard on the same gel. Bands of interest were cut and placed in eppendorf tubes in 30 µl of 1% acetic acid solution and stored at −20C until MS/MS analysis.

Protein digestion

Excised gel bands were treated to remove salts, buffers and detergent using 3 washes of 50 mM NH_4HCO_3 intercalated with gel shrinkages in 50% acetonitrile (ACN). Disulfide bonds were disrupted with 20 mM DTT at 56°C for 30 min and subsequently alkylated in 55 mM chloroacetamide for 30 min at room temperature. A last wash with 50% ACN and 50 mM NH_4HCO_3 was performed before addition of 50 ng of trypsin (Promega Sequencing Grade) for an overnight digestion on an Eppendorf Thermomix at 30°C. Peptides were then extracted using 2 washes of 1% formic acid intercalated with gel shrinkages in 50% ACN. The two washes were pooled and evaporated before analysis.

LC-MS/MS

20% of each sample was analyzed in LC-MS-MS using an Ultimate 3000 Rapid Separation liquid chromatographic system coupled to an Orbitrap Fusion mass spectrometer (both from Thermo Fisher Scientific). Peptides were directly loaded on a C_{18} reverse phase analytical column (2 µm particle size, 100 Å pore size, 75 µm internal diameter, 50 cm length) with a 45 min effective gradient from 99% A (0.1% formic acid and 100% H2O) to 50% B (80% ACN, 0.085% formic acid and 20% H2O). The Orbitrap Fusion mass spectrometer acquired data throughout the elution process and operated in a data dependent scheme with full MS scans acquired with the orbitrap, followed by stepped HCD MS/MS (top speed mode in 3 s) on the most abundant ions detected in the MS scan. Mass spectrometer settings were: full MS (AGC: $4.0E^5$, resolution: 120,000, m/z range 350–1500, maximum ion injection time: 60 ms); MS/MS was performed using Stepped HCD Normalized Collision Energy at 30 plus and minus 5%, Orbitrap resolution was set at 17500, intensity threshold: $1.0E^4$, isolation window: 1.6 m/z, dynamic exclusion time setting: 30 s, AGC Target: $1.0E^4$ and maximum injection time: 100 ms). The fragmentation was permitted of precursor with a charge state of 2 to 4. The software used to generate. mgf files is Proteome discoverer 1.4.

Peptide identification

Mass list were used to perform comparison of MS/MS experimental peak lists with the *Homo sapiens* taxon of the Swiss-Prot database (November 2016, 20,204 sequences) using Mascot version 2.5.1 (*Perkins et al., 1999*). The cleavage specificity set was the trypsin with maximum four missed cleavages. The precursor mass tolerance was set to 4 ppm and the MS/MS mass tolerance to 0.55 Da. Cystein carbamidomethylation was set as a constant modification while methionine oxidation, tyrosine, serine and threonine phosphorylation were set as variable modification. With these settings, peptide identifications were considered as valid whenever their scores reached a minimum of 23, thus meeting the *p*-values criteria less than 0.05.

Additional information

Author contributions

PJ, Conceptualization, Data curation, Formal analysis, Validation, Investigation, Methodology, Writing—original draft; AN, Conceptualization, Data curation, Investigation, Methodology; RTP, Data curation, Investigation, Methodology; CC, Investigation, Methodology; EB, Data curation, Formal analysis, Investigation, Methodology; TK, Resources, Methodology; PM, Conceptualization, Data curation, Formal analysis, Investigation; FG, Conceptualization, Data curation, Formal analysis, Investigation, Methodology, Writing—review and editing; SM, Funding acquisition, Writing—original draft, Project administration; AB, Conceptualization, Resources, Data curation, Formal analysis, Supervision, Funding acquisition, Validation, Investigation, Methodology, Writing—original draft, Project administration, Writing—review and editing

Author ORCIDs

Arnaud Besson, http://orcid.org/0000-0002-9599-3943

References

Arthur WT, Burridge K. 2001. RhoA inactivation by p190RhoGAP regulates cell spreading and migration by promoting membrane protrusion and polarity. *Molecular Biology of the Cell* **12**:2711–2720. doi: 10.1091/mbc.12.9.2711, PMID: 11553710

Baldassarre G, Belletti B, Nicoloso MS, Schiappacassi M, Vecchione A, Spessotto P, Morrione A, Canzonieri V, Colombatti A. 2005. p27(Kip1)-stathmin interaction influences sarcoma cell migration and invasion. *Cancer Cell* **7**:51–63. doi: 10.1016/j.ccr.2004.11.025, PMID: 15652749

Belletti B, Pellizzari I, Berton S, Fabris L, Wolf K, Lovat F, Schiappacassi M, D'Andrea S, Nicoloso MS, Lovisa S, Sonego M, Defilippi P, Vecchione A, Colombatti A, Friedl P, Baldassarre G. 2010. p27kip1 controls cell morphology and motility by regulating microtubule-dependent lipid raft recycling. *Molecular and Cellular Biology* **30**:2229–2240. doi: 10.1128/MCB.00723-09, PMID: 20194624

Besson A, Assoian RK, Roberts JM. 2004a. Regulation of the cytoskeleton: an oncogenic function for CDK inhibitors? *Nature Reviews Cancer* **4**:948–955. doi: 10.1038/nrc1501, PMID: 15573116

Besson A, Gurian-West M, Schmidt A, Hall A, Roberts JM. 2004b. p27Kip1 modulates cell migration through the regulation of RhoA activation. *Genes & Development* **18**:862–876. doi: 10.1101/gad.1185504, PMID: 15078817

Besson A, Gurian-West M, Chen X, Kelly-Spratt KS, Kemp CJ, Roberts JM. 2006. A pathway in quiescent cells that controls p27Kip1 stability, subcellular localization, and tumor suppression. *Genes & Development* **20**:47–64. doi: 10.1101/gad.1384406, PMID: 16391232

Besson A, Hwang HC, Cicero S, Donovan SL, Gurian-West M, Johnson D, Clurman BE, Dyer MA, Roberts JM. 2007. Discovery of an oncogenic activity in p27Kip1 that causes stem cell expansion and a multiple tumor phenotype. *Genes & Development* **21**:1731–1746. doi: 10.1101/gad.1556607, PMID: 17626791

Besson A, Dowdy SF, Roberts JM. 2008. CDK inhibitors: cell cycle regulators and beyond. *Developmental Cell* **14**:159–169. doi: 10.1016/j.devcel.2008.01.013, PMID: 18267085

Bian Y, Song C, Cheng K, Dong M, Wang F, Huang J, Sun D, Wang L, Ye M, Zou H. 2014. An enzyme assisted RP-RPLC approach for in-depth analysis of human liver phosphoproteome. *Journal of Proteomics* **96**:253–262. doi: 10.1016/j.jprot.2013.11.014, PMID: 24275569

Bisht S, Nolting J, Schütte U, Haarmann J, Jain P, Shah D, Brossart P, Flaherty P, Feldmann G. 2015. Cyclin-Dependent kinase 5 (CDK5) Controls melanoma cell motility, invasiveness, and metastatic Spread-Identification of a promising novel therapeutic target. *Translational Oncology* **8**:295–307. doi: 10.1016/j.tranon.2015.06.002, PMID: 26310376

Boehm M, Yoshimoto T, Crook MF, Nallamshetty S, True A, Nabel GJ, Nabel EG. 2002. A growth factor-dependent nuclear kinase phosphorylates p27$^{(Kip1)}$ and regulates cell cycle progression. *The EMBO Journal* **21**:3390–3401. doi: 10.1093/emboj/cdf343, PMID: 12093740

Castro-Castro A, Janke C, Montagnac G, Paul-Gilloteaux P, Chavrier P. 2012. ATAT1/MEC-17 acetyltransferase and HDAC6 deacetylase control a balance of acetylation of alpha-tubulin and cortactin and regulate MT1-MMP trafficking and breast tumor cell invasion. *European Journal of Cell Biology* **91**:950–960. doi: 10.1016/j.ejcb.2012.07.001, PMID: 22902175

Chen L, Giorgianni F, Beranova-Giorgianni S. 2010. Characterization of the phosphoproteome in LNCaP prostate Cancer cells by in-gel isoelectric focusing and tandem mass spectrometry. *Journal of Proteome Research* **9**:174–178. doi: 10.1021/pr900338q, PMID: 20044836

Cheng Y, Lu J, Chen G, Ardekani GS, Rotte A, Martinka M, Xu X, McElwee KJ, Zhang G, Zhou Y. 2015. Stage-specific prognostic biomarkers in melanoma. *Oncotarget* **6**:4180–4189. doi: 10.18632/oncotarget.2907, PMID: 25784655

Chong C, Tan L, Lim L, Manser E. 2001. The mechanism of PAK activation. autophosphorylation events in both regulatory and kinase domains control activity. *Journal of Biological Chemistry* **276**:17347–17353. doi: 10.1074/jbc.M009316200, PMID: 11278486

Chu IM, Hengst L, Slingerland JM. 2008. The cdk inhibitor p27 in human Cancer: prognostic potential and relevance to anticancer therapy. *Nature Reviews Cancer* **8**:253–267. doi: 10.1038/nrc2347, PMID: 18354415

Clark ES, Whigham AS, Yarbrough WG, Weaver AM. 2007. Cortactin is an essential regulator of matrix metalloproteinase secretion and extracellular matrix degradation in invadopodia. *Cancer Research* **67**:4227–4235. doi: 10.1158/0008-5472.CAN-06-3928, PMID: 17483334

Connor MK, Kotchetkov R, Cariou S, Resch A, Lupetti R, Beniston RG, Melchior F, Hengst L, Slingerland JM. 2003. CRM1/Ran-mediated nuclear export of p27(Kip1) involves a nuclear export signal and links p27 export and proteolysis. *Molecular Biology of the Cell* **14**:201–213. doi: 10.1091/mbc.E02-06-0319, PMID: 12529437

Cox EA, Sastry SK, Huttenlocher A. 2001. Integrin-mediated adhesion regulates cell polarity and membrane protrusion through the rho family of GTPases. *Molecular Biology of the Cell* **12**:265–277. doi: 10.1091/mbc.12.2.265, PMID: 11179414

Denicourt C, Saenz CC, Datnow B, Cui XS, Dowdy SF. 2007. Relocalized p27Kip1 tumor suppressor functions as a cytoplasmic metastatic oncogene in melanoma. *Cancer Research* **67**:9238–9243. doi: 10.1158/0008-5472.CAN-07-1375, PMID: 17909030

Di Martino J, Henriet E, Ezzoukhry Z, Goetz JG, Moreau V, Saltel F. 2016. The microenvironment controls invadosome plasticity. *Journal of Cell Science* **129**:1759–1768. doi: 10.1242/jcs.182329, PMID: 27029343

Fero ML, Rivkin M, Tasch M, Porter P, Carow CE, Firpo E, Polyak K, Tsai LH, Broudy V, Perlmutter RM, Kaushansky K, Roberts JM. 1996. A syndrome of Multiorgan Hyperplasia with features of gigantism,

Tumorigenesis, and female sterility in p27(Kip1)-deficient mice. *Cell* **85**:733–744. doi: 10.1016/S0092-8674(00)81239-8, PMID: 8646781

Fero ML, Randel E, Gurley KE, Roberts JM, Kemp CJ. 1998. The murine gene p27Kip1 is haplo-insufficient for tumour suppression. *Nature* **396**:177–180. doi: 10.1038/24179, PMID: 9823898

Friedl P, Wolf K. 2003. Tumour-cell invasion and migration: diversity and escape mechanisms. *Nature Reviews Cancer* **3**:362–374. doi: 10.1038/nrc1075, PMID: 12724734

Galea CA, Nourse A, Wang Y, Sivakolundu SG, Heller WT, Kriwacki RW. 2008. Role of intrinsic flexibility in signal transduction mediated by the cell cycle regulator, p27 Kip1. *Journal of Molecular Biology* **376**:827–838. doi: 10.1016/j.jmb.2007.12.016, PMID: 18177895

Gao Y, Dickerson JB, Guo F, Zheng J, Zheng Y. 2004. Rational design and characterization of a rac GTPase-specific small molecule inhibitor. *PNAS* **101**:7618–7623. doi: 10.1073/pnas.0307512101, PMID: 15128949

Godin JD, Thomas N, Laguesse S, Malinouskaya L, Close P, Malaise O, Purnelle A, Raineteau O, Campbell K, Fero M, Moonen G, Malgrange B, Chariot A, Metin C, Besson A, Nguyen L. 2012. p27(Kip1) is a microtubule-associated protein that promotes microtubule polymerization during neuron migration. *Developmental Cell* **23**:729–744. doi: 10.1016/j.devcel.2012.08.006, PMID: 23022035

Gui P, Labrousse A, Van Goethem E, Besson A, Maridonneau-Parini I, Le Cabec V, Goethem, E VAN, Cabec LE, V. 2014. Rho/ROCK pathway inhibition by the CDK inhibitor p27(kip1) participates in the onset of macrophage 3D-mesenchymal migration. *Journal of Cell Science* **127**:4009–4023. doi: 10.1242/jcs.150987, PMID: 25015295

Hydbring P, Malumbres M, Sicinski P. 2016. Non-canonical functions of cell cycle cyclins and cyclin-dependent kinases. *Nature Reviews Molecular Cell Biology* **17**:280–292. doi: 10.1038/nrm.2016.27, PMID: 27033256

Ishida N, Hara T, Kamura T, Yoshida M, Nakayama K, Nakayama KI. 2002. Phosphorylation of p27Kip1 on serine 10 is required for its binding to CRM1 and nuclear export. *Journal of Biological Chemistry* **277**:14355–14358. doi: 10.1074/jbc.C100762200, PMID: 11889117

Jeannot P, Callot C, Baer R, Duquesnes N, Guerra C, Guillermet-Guibert J, Bachs O, Besson A. 2015. Loss of p27Kip1 promotes metaplasia in the pancreas via the regulation of Sox9 expression. *Oncotarget* **6**:35880–35892. doi: 10.18632/oncotarget.5770, PMID: 26416424

Jin X, Jin X, Sohn YW, Yin J, Kim SH, Joshi K, Nam DH, Nakano I, Kim H. 2013. Blockade of EGFR signaling promotes glioma stem-like cell invasiveness by abolishing ID3-mediated inhibition of p27(KIP1) and MMP3 expression. *Cancer Letters* **328**:235–242. doi: 10.1016/j.canlet.2012.09.005, PMID: 23022473

Kandoth C, McLellan MD, Vandin F, Ye K, Niu B, Lu C, Xie M, Zhang Q, McMichael JF, Wyczalkowski MA, Leiserson MD, Miller CA, Welch JS, Walter MJ, Wendl MC, Ley TJ, Wilson RK, Raphael BJ, Ding L. 2013. Mutational landscape and significance across 12 major Cancer types. *Nature* **502**:333–339. doi: 10.1038/nature12634, PMID: 24132290

Katsube T, Togashi S, Hashimoto N, Ogiu T, Tsuji H. 2004. Filamentous actin binding ability of cortactin isoforms is responsible for their cell-cell junctional localization in epithelial cells. *Archives of Biochemistry and Biophysics* **427**:79–90. doi: 10.1016/j.abb.2004.04.015, PMID: 15178490

Kawauchi T, Chihama K, Nabeshima Y, Hoshino M. 2006. Cdk5 phosphorylates and stabilizes p27kip1 contributing to actin organization and cortical neuronal migration. *Nature Cell Biology* **8**:17–26. doi: 10.1038/ncb1338, PMID: 16341208

Kirkbride KC, Sung BH, Sinha S, Weaver AM. 2011. Cortactin: a multifunctional regulator of cellular invasiveness. *Cell Adhesion & Migration* **5**:187–198. doi: 10.4161/cam.5.2.14773, PMID: 21258212

Kiyokawa H, Kineman RD, Manova-Todorova KO, Soares VC, Hoffman ES, Ono M, Khanam D, Hayday AC, Frohman LA, Koff A. 1996. Enhanced growth of mice lacking the cyclin-dependent kinase inhibitor function of p27(Kip1). *Cell* **85**:721–732. doi: 10.1016/S0092-8674(00)81238-6, PMID: 8646780

Klammer M, Kaminski M, Zedler A, Oppermann F, Blencke S, Marx S, Müller S, Tebbe A, Godl K, Schaab C. 2012. Phosphosignature predicts dasatinib response in non-small cell lung Cancer. *Molecular & Cellular Proteomics* **11**:651–668. doi: 10.1074/mcp.M111.016410, PMID: 22617229

Lacy ER, Filippov I, Lewis WS, Otieno S, Xiao L, Weiss S, Hengst L, Kriwacki RW. 2004. p27 binds cyclin-CDK complexes through a sequential mechanism involving binding-induced protein folding. *Nature Structural & Molecular Biology* **11**:358–364. doi: 10.1038/nsmb746, PMID: 15024385

Lacy ER, Wang Y, Post J, Nourse A, Webb W, Mapelli M, Musacchio A, Siuzdak G, Kriwacki RW. 2005. Molecular basis for the specificity of p27 toward cyclin-dependent kinases that regulate cell division. *Journal of Molecular Biology* **349**:764–773. doi: 10.1016/j.jmb.2005.04.019, PMID: 15890360

Larrea MD, Hong F, Wander SA, da Silva TG, Helfman D, Lannigan D, Smith JA, Slingerland JM. 2009. RSK1 drives p27Kip1 phosphorylation at T198 to promote RhoA inhibition and increase cell motility. *PNAS* **106**:9268–9273. doi: 10.1073/pnas.0805057106, PMID: 19470470

Lee MH, Nikolic M, Baptista CA, Lai E, Tsai LH, Massagué J. 1996. The brain-specific activator p35 allows Cdk5 to escape inhibition by p27Kip1 in neurons. *PNAS* **93**:3259–3263. doi: 10.1073/pnas.93.8.3259, PMID: 8622924

Li Z, Jiao X, Wang C, Ju X, Lu Y, Yuan L, Lisanti MP, Katiyar S, Pestell RG. 2006. Cyclin D1 induction of cellular migration requires p27(KIP1). *Cancer Research* **66**:9986–9994. doi: 10.1158/0008-5472.CAN-06-1596, PMID: 17047061

Li H, Collado M, Villasante A, Matheu A, Lynch CJ, Cañamero M, Rizzoti K, Carneiro C, Martínez G, Vidal A, Lovell-Badge R, Serrano M. 2012. p27(Kip1) directly represses Sox2 during embryonic stem cell differentiation. *Cell Stem Cell* **11**:845–852. doi: 10.1016/j.stem.2012.09.014, PMID: 23217425

Liang J, Zubovitz J, Petrocelli T, Kotchetkov R, Connor MK, Han K, Lee JH, Ciarallo S, Catzavelos C, Beniston R, Franssen E, Slingerland JM. 2002. PKB/Akt phosphorylates p27, impairs nuclear import of p27 and opposes p27-mediated G1 arrest. *Nature Medicine* **8**:1153–1160. doi: 10.1038/nm761, PMID: 12244302

Liang J, Shao SH, Xu ZX, Hennessy B, Ding Z, Larrea M, Kondo S, Dumont DJ, Gutterman JU, Walker CL, Slingerland JM, Mills GB. 2007. The energy sensing LKB1-AMPK pathway regulates p27(kip1) phosphorylation mediating the decision to enter autophagy or apoptosis. *Nature Cell Biology* **9**:218–224. doi: 10.1038/ncb1537, PMID: 17237771

Licciulli S, Maksimoska J, Zhou C, Troutman S, Kota S, Liu Q, Duron S, Campbell D, Chernoff J, Field J, Marmorstein R, Kissil JL. 2013. FRAX597, a small molecule inhibitor of the p21-activated kinases, inhibits tumorigenesis of neurofibromatosis type 2 (NF2)-associated schwannomas. *Journal of Biological Chemistry* **288**:29105–29114. doi: 10.1074/jbc.M113.510933, PMID: 23960073

Lin TC, Tsai LH, Chou MC, Chen CY, Lee H. 2016. Association of cytoplasmic p27 expression with an unfavorable response to cisplatin-based chemotherapy and poor outcomes in non-small cell lung Cancer. *Tumor Biology* **37**:4017–4023. doi: 10.1007/s13277-015-4272-7, PMID: 26482622

Linder S, Wiesner C, Himmel M. 2011. Degrading devices: invadosomes in proteolytic cell invasion. *Annual Review of Cell and Developmental Biology* **27**:185–211. doi: 10.1146/annurev-cellbio-092910-154216, PMID: 21 801014

Lu W, Katz S, Gupta R, Mayer BJ. 1997. Activation of pak by membrane localization mediated by an SH3 domain from the adaptor protein nck. *Current Biology* **7**:85–94. doi: 10.1016/S0960-9822(06)00052-2, PMID: 9024622

Lu W, Mayer BJ. 1999. Mechanism of activation of Pak1 kinase by membrane localization. *Oncogene* **18**:797–806. doi: 10.1038/sj.onc.1202361, PMID: 9989831

MacGrath SM, Koleske AJ. 2012. Cortactin in cell migration and Cancer at a glance. *Journal of Cell Science* **125**:1621–1626. doi: 10.1242/jcs.093781, PMID: 22566665

Malliri A, Ten KJP, Olivio C, Collard JG. 2000. Determination of the activity of Rho-like GTPases in cells. *Methods in Molecular Biology* **189**:99–109. doi: 10.1385/1-59259-281-3:099

Mertins P, Yang F, Liu T, Mani DR, Petyuk VA, Gillette MA, Clauser KR, Qiao JW, Gritsenko MA, Moore RJ, Levine DA, Townsend R, Erdmann-Gilmore P, Snider JE, Davies SR, Ruggles KV, Fenyo D, Kitchens RT, Li S, Olvera R, et al. 2014. Ischemia in tumors induces early and sustained phosphorylation changes in stress kinase pathways but does not affect global protein levels. *Molecular & Cellular Proteomics* **13**:1690–1704. doi: 10.1074/mcp.M113.036392, PMID: 24719451

Mertins P, Mani DR, Ruggles KV, Gillette MA, Clauser KR, Wang P, Wang X, Qiao JW, Cao S, Petralia F, Kawaler E, Mundt F, Krug K, Tu Z, Lei JT, Gatza ML, Wilkerson M, Perou CM, Yellapantula V, Huang KL, et al. 2016. Proteogenomics connects somatic mutations to signalling in breast Cancer. *Nature* **534**:55–62. doi: 10.1038/nature18003, PMID: 27251275

Min YH, Cheong JW, Kim JY, Eom JI, Lee ST, Hahn JS, Ko YW, Lee MH. 2004. Cytoplasmic mislocalization of p27Kip1 protein is associated with constitutive phosphorylation of akt or protein kinase B and poor prognosis in acute myelogenous leukemia. *Cancer Research* **64**:5225–5231. doi: 10.1158/0008-5472.CAN-04-0174, PMID: 15289327

Moshfegh Y, Bravo-Cordero JJ, Miskolci V, Condeelis J, Hodgson L. 2014. A Trio-Rac1-Pak1 signalling Axis drives invadopodia disassembly. *Nature Cell Biology* **16**:574–586. doi: 10.1038/ncb2972, PMID: 24859002

Murphy DA, Courtneidge SA. 2011. The 'ins' and 'outs' of podosomes and invadopodia: characteristics, formation and function. *Nature Reviews Molecular Cell Biology* **12**:413–426. doi: 10.1038/nrm3141, PMID: 216 97900

Nagahara H, Vocero-Akbani AM, Snyder EL, Ho A, Latham DG, Lissy NA, Becker-Hapak M, Ezhevsky SA, Dowdy SF. 1998. Transduction of full-length TAT fusion proteins into mammalian cells: tat-p27kip1 induces cell migration. *Nature Medicine* **4**:1449–1452. doi: 10.1038/4042, PMID: 9846587

Nakayama K, Ishida N, Shirane M, Inomata A, Inoue T, Shishido N, Horii I, Loh DY, Nakayama K. 1996. Mice lacking p27(Kip1) display increased body size, multiple organ Hyperplasia, retinal dysplasia, and pituitary tumors. *Cell* **85**:707–720. doi: 10.1016/S0092-8674(00)81237-4, PMID: 8646779

Ndubaku CO, Crawford JJ, Drobnick J, Aliagas I, Campbell D, Dong P, Dornan LM, Duron S, Epler J, Gazzard L, Heise CE, Hoeflich KP, Jakubiak D, La H, Lee W, Lin B, Lyssikatos JP, Maksimoska J, Marmorstein R, Murray LJ, et al. 2015. Design of selective PAK1 inhibitor G-5555: improving properties by employing an unorthodox Low-pK a polar moiety. *ACS Medicinal Chemistry Letters* **6**:1241–1246. doi: 10.1021/acsmedchemlett.5b00398, PMID: 26713112

Nguyen L, Besson A, Heng JI, Schuurmans C, Teboul L, Parras C, Philpott A, Roberts JM, Guillemot F. 2006. p27kip1 independently promotes neuronal differentiation and migration in the cerebral cortex. *Genes & Development* **20**:1511–1524. doi: 10.1101/gad.377106, PMID: 16705040

Nickeleit I, Zender S, Sasse F, Geffers R, Brandes G, Sörensen I, Steinmetz H, Kubicka S, Carlomagno T, Menche D, Gütgemann I, Buer J, Gossler A, Manns MP, Kalesse M, Frank R, Malek NP. 2008. Argyrin a reveals a critical role for the tumor suppressor protein p27(kip1) in mediating antitumor activities in response to proteasome inhibition. *Cancer Cell* **14**:23–35. doi: 10.1016/j.ccr.2008.05.016, PMID: 18598941

Olsen JV, Vermeulen M, Santamaria A, Kumar C, Miller ML, Jensen LJ, Gnad F, Cox J, Jensen TS, Nigg EA, Brunak S, Mann M. 2010. Quantitative phosphoproteomics reveals widespread full phosphorylation site occupancy during mitosis. *Science Signaling* **3**:ra3. doi: 10.1126/scisignal.2000475, PMID: 20068231

Ong CC, Gierke S, Pitt C, Sagolla M, Cheng CK, Zhou W, Jubb AM, Strickland L, Schmidt M, Duron SG, Campbell DA, Zheng W, Dehdashti S, Shen M, Yang N, Behnke ML, Huang W, McKew JC, Chernoff J, Forrest WF, et al. 2015. Small molecule inhibition of group I p21-activated kinases in breast Cancer induces apoptosis and potentiates the activity of microtubule stabilizing agents. *Breast Cancer Research* **17**:59. doi: 10.1186/s13058-015-0564-5, PMID: 25902869

Oser M, Yamaguchi H, Mader CC, Bravo-Cordero JJ, Arias M, Chen X, Desmarais V, van Rheenen J, Koleske AJ, Condeelis J. 2009. Cortactin regulates cofilin and N-WASp activities to control the stages of invadopodium assembly and maturation. *The Journal of Cell Biology* **186**:571–587. doi: 10.1083/jcb.200812176, PMID: 1 9704022

Oser M, Mader CC, Gil-Henn H, Magalhaes M, Bravo-Cordero JJ, Koleske AJ, Condeelis J. 2010. Specific tyrosine phosphorylation sites on cortactin regulate Nck1-dependent actin polymerization in invadopodia. *Journal of Cell Science* **123**:3662–3673. doi: 10.1242/jcs.068163, PMID: 20971703

Ou L, Waddell MB, Kriwacki RW. 2012. Mechanism of cell cycle entry mediated by the intrinsically disordered protein p27(Kip1). *ACS Chemical Biology* **7**:678–682. doi: 10.1021/cb200487h, PMID: 22276948

Papakonstanti EA, Ridley AJ, Vanhaesebroeck B. 2007. The p110delta isoform of PI 3-kinase negatively controls RhoA and PTEN. *The EMBO Journal* **26**:3050–3061. doi: 10.1038/sj.emboj.7601763, PMID: 17581634

Perkins DN, Pappin DJ, Creasy DM, Cottrell JS. 1999. Probability-based protein identification by searching sequence databases using mass spectrometry data. *Electrophoresis* **20**:3551–3567. doi: 10.1002/(SICI)1522-2683(19991201)20:18<3551::AID-ELPS3551>3.0.CO;2-2, PMID: 10612281

Petrie RJ, Yamada KM. 2016. Multiple mechanisms of 3D migration: the origins of plasticity. *Current Opinion in Cell Biology* **42**:7–12. doi: 10.1016/j.ceb.2016.03.025, PMID: 27082869

Pippa R, Espinosa L, Gundem G, García-Escudero R, Dominguez A, Orlando S, Gallastegui E, Saiz C, Besson A, Pujol MJ, López-Bigas N, Paramio JM, Bigas A, Bachs O. 2012. p27Kip1 represses transcription by direct interaction with p130/E2F4 at the promoters of target genes. *Oncogene* **31**:4207–4220. doi: 10.1038/onc.2011. 582, PMID: 22179826

Quintavalle M, Elia L, Price JH, Heynen-Genel S, Courtneidge SA. 2011. A cell-based high-content screening assay reveals activators and inhibitors of Cancer cell invasion. *Science Signaling* **4**:ra49. doi: 10.1126/scisignal. 2002032, PMID: 21791703

Ren XD, Kiosses WB, Sieg DJ, Otey CA, Schlaepfer DD, Schwartz MA. 2000. Focal adhesion kinase suppresses rho activity to promote focal adhesion turnover. *Journal of Cell Science* **113 (Pt 20**:3637–3678. PMID: 11017 882

Rinschen MM, Yu MJ, Wang G, Boja ES, Hoffert JD, Pisitkun T, Knepper MA. 2010. Quantitative phosphoproteomic analysis reveals vasopressin V2-receptor-dependent signaling pathways in renal collecting duct cells. *PNAS* **107**:3882–3887. doi: 10.1073/pnas.0910646107, PMID: 20139300

Rodier G, Montagnoli A, Di Marcotullio L, Coulombe P, Draetta GF, Pagano M, Meloche S. 2001. p27 cytoplasmic localization is regulated by phosphorylation on Ser10 and is not a prerequisite for its proteolysis. *The EMBO Journal* **20**:6672–6682. doi: 10.1093/emboj/20.23.6672, PMID: 11726503

Spector DL. 1997. Isolation of fibroblasts. Goldman R, Leinwand L. *Cells: A Laboratory Manual.* New York: Cold Spring Harbor Laboratory Press.

Sahai E, Olson MF, Marshall CJ. 2001. Cross-talk between ras and rho signalling pathways in transformation favours proliferation and increased motility. *The EMBO Journal* **20**:755–766. doi: 10.1093/emboj/20.4.755, PMID: 1117 9220

Sahai E, Marshall CJ. 2003. Differing modes of tumour cell invasion have distinct requirements for rho/ROCK signalling and extracellular proteolysis. *Nature Cell Biology* **5**:711–719. doi: 10.1038/ncb1019, PMID: 12844144

Sander EE, van Delft S, ten Klooster JP, Reid T, van der Kammen RA, Michiels F, Collard JG. 1998. Matrix-dependent Tiam1/Rac signaling in epithelial cells promotes either cell-cell adhesion or cell migration and is regulated by phosphatidylinositol 3-kinase. *The Journal of Cell Biology* **143**:1385–1398. doi: 10.1083/jcb.143.5. 1385, PMID: 9832565

Seals DF, Azucena EF, Pass I, Tesfay L, Gordon R, Woodrow M, Resau JH, Courtneidge SA, Pass JR, Resau M, J. H. 2005. The adaptor protein Tks5/Fish is required for podosome formation and function, and for the protease-driven invasion of Cancer cells. *Cancer Cell* **7**:155–165. doi: 10.1016/j.ccr.2005.01.006, PMID: 15710328

See WL, Heinberg AR, Holland EC, Resh MD. 2010. p27 deficiency is associated with migration defects in PDGF-expressing gliomas in vivo. *Cell Cycle* **9**:1562–1567. doi: 10.4161/cc.9.8.11259, PMID: 20404478

Serres MP, Zlotek-Zlotkiewicz E, Concha C, Gurian-West M, Daburon V, Roberts JM, Besson A. 2011. Cytoplasmic p27 is oncogenic and cooperates with ras both in vivo and in vitro. *Oncogene* **30**:2846–2858. doi: 10.1038/onc.2011.9, PMID: 21317921

Serres MP, Kossatz U, Chi Y, Roberts JM, Malek NP, Besson A. 2012. p27(Kip1) controls cytokinesis via the regulation of Citron kinase activation. *Journal of Clinical Investigation* **122**:844–858. doi: 10.1172/JCI60376, PMID: 22293177

Sethi N, Kang Y. 2011. Unravelling the complexity of metastasis - molecular understanding and targeted therapies. *Nature Reviews Cancer* **11**:735–748. doi: 10.1038/nrc3125, PMID: 21941285

Sharma SS, Pledger WJ. 2016. The non-canonical functions of p27(Kip1) in normal and tumor biology. *Cell Cycle* **15**:1–13. doi: 10.1080/15384101.2016.1157238, PMID: 27082696

Shvetsov A, Berkane E, Chereau D, Dominguez R, Reisler E. 2009. The actin-binding domain of cortactin is dynamic and unstructured and affects lateral and longitudinal contacts in F-actin. *Cell Motility and the Cytoskeleton* **66**:90–98. doi: 10.1002/cm.20328, PMID: 19089942

Sun Y, Sun J, Lungchukiet P, Quarni W, Yang S, Zhang X, Bai W. 2015. Fe65 suppresses breast Cancer cell migration and invasion through Tip60 mediated cortactin acetylation. *Scientific Reports* **5**:11529. doi: 10.1038/ srep11529, PMID: 26166158

Vial E, Sahai E, Marshall CJ. 2003. ERK-MAPK signaling coordinately regulates activity of Rac1 and RhoA for tumor cell motility. *Cancer Cell* **4**:67–79. doi: 10.1016/S1535-6108(03)00162-4, PMID: 12892714

Vidal C, Geny B, Melle J, Jandrot-Perrus M, Fontenay-Roupie M. 2002. Cdc42/Rac1-dependent activation of the p21-activated kinase (PAK) regulates human platelet lamellipodia spreading: implication of the cortical-actin binding protein cortactin. *Blood* **100**:4462–4469. doi: 10.1182/blood.V100.13.4462, PMID: 12453877

Weaver AM, Heuser JE, Karginov AV, Lee WL, Parsons JT, Cooper JA. 2002. Interaction of cortactin and N-WASp with Arp2/3 complex. *Current Biology* **12**:1270–1278. doi: 10.1016/S0960-9822(02)01035-7, PMID: 12176354

Webb BA, Eves R, Crawley SW, Zhou S, Côté GP, Mak AS. 2005. PAK1 induces podosome formation in A7r5 vascular smooth muscle cells in a PAK-interacting exchange factor-dependent manner. *AJP: Cell Physiology* **289**:C898–C907. doi: 10.1152/ajpcell.00095.2005, PMID: 15944209

Webb BA, Zhou S, Eves R, Shen L, Jia L, Mak AS. 2006. Phosphorylation of cortactin by p21-activated kinase. *Archives of Biochemistry and Biophysics* **456**:183–193. doi: 10.1016/j.abb.2006.06.011, PMID: 16854367

Wiśniewski JR, Nagaraj N, Zougman A, Gnad F, Mann M. 2010. Brain phosphoproteome obtained by a FASP-based method reveals plasma membrane protein topology. *Journal of Proteome Research* **9**:3280–3289. doi: 10.1021/pr1002214, PMID: 20415495

Wu FY, Wang SE, Sanders ME, Shin I, Rojo F, Baselga J, Arteaga CL. 2006. Reduction of cytosolic p27(Kip1) inhibits Cancer cell motility, survival, and tumorigenicity. *Cancer Research* **66**:2162–2172. doi: 10.1158/0008-5472.CAN-05-3304, PMID: 16489017

Yang J, Liao D, Wang Z, Liu F, Wu G. 2011. Mammalian target of rapamycin signaling pathway contributes to glioma progression and patients' Prognosis. *Journal of Surgical Research* **168**:97–102. doi: 10.1016/j.jss.2009.06.025

Zhang X, Yuan Z, Zhang Y, Yong S, Salas-Burgos A, Koomen J, Olashaw N, Parsons JT, Yang XJ, Dent SR, Yao TP, Lane WS, Seto E. 2007. HDAC6 modulates cell motility by altering the acetylation level of cortactin. *Molecular Cell* **27**:197–213. doi: 10.1016/j.molcel.2007.05.033, PMID: 17643370

Zhang Y, Zhang M, Dong H, Yong S, Li X, Olashaw N, Kruk PA, Cheng JQ, Bai W, Chen J, Nicosia SV, Zhang X. 2009. Deacetylation of cortactin by SIRT1 promotes cell migration. *Oncogene* **28**:445–460. doi: 10.1038/onc.2008.388, PMID: 18850005

Zhao D, Besser AH, Wander SA, Sun J, Zhou W, Wang B, Ince T, Durante MA, Guo W, Mills G, Theodorescu D, Slingerland J. 2015. Cytoplasmic p27 promotes epithelial-mesenchymal transition and tumor metastasis via STAT3-mediated Twist1 upregulation. *Oncogene* **34**:5447–5459. doi: 10.1038/onc.2014.473, PMID: 25684140